2011

Diffusion Model and Experimental Verification of Interfacial Multiple Phase Growth in a Thermal Energy Storage Binary System

Bandar Abdulrahman Alzahrani
Lehigh University

Diffusion Model and Experimental Verification of Interfacial Multiple Phase Growth in a Thermal Energy Storage Binary System

By

(Bandar A. Alzahrani)

A Thesis

Presented to the Graduate and Research Committee

of Lehigh University

in Candidacy for the Degree of

Master of Science

in

Mechanical Engineering and Mechanics

Lehigh University

Bethlehem, PA

(September, 2011)

September 2011

This thesis is accepted and approved in partial fulfillment of the requirements for the Master of Science.

_____

Date

_____

Thesis Advisor: Wojciech Z. Misiolek

_____

Co-advisor: Alparslan Oztekin

_____

Chairperson of Department: D. Gary Harlow

Table of Contents

ACKNOWLEDGMENTS

First of all, all praise due to Allah for his blessing and giving me strength and health. Secondly, thanks to my parents whose gave their love, their life and their continual support. I dedicate this work for them. May Allah bless my parents and give me the strength and health to serve them as I should.

Special thanks to my lovely wife Nada and my daughters for their love, support, and patient during my study. In particular, my wife Nada; without your continuous support and encouragement, this work will be difficult to achieve. So thanks from deep of my heart. I would like to thank my brothers and sisters for their support and prayers.

Many thanks to my friend Nabeel; we have spent a great time together during which a lot of obstacles that have proved the close relationship we have. I wish from Allah to help you achieve your dreams.

I would like to express my gratitude and respect to my research advisor, Professor Wojciech Z. Misiolek, and my research co-advisor, Professor Alparslan Oztekin, for their guidance and endless support in this thesis, for their inspiration, motivations and encouragement throughout my research.

My gratitude to Joseph Sabol for his assistance of preparing the samples and taking the optical microscopy images for this research and his valuable discussion and editing of the paper.

Thanks to my colleagues members in the Institute for Metal Forming (IMF), for their support and fruitful discussions.

Thanks to Lehigh University to give me the opportunity to be one of its graduate students. Thanks to Department of Energy for their financial support to this research.

Finally, I also would like to thank the government of Saudi Arabia represented by the Minister of Higher Education for the financial support I had throughout my master degree study.

LIST OF TABLES

LIST OF FIGURES

ABSTRACT

Diffusion in binary systems with multiple solid phases was modeled analytically using a self-similar solution. A system of coupled nonlinear equations predicting the location of the propagating front was solved numerically for the values of propagation rate constants. The Al-Zn binary system was studied theoretically while both Ni-Zn and Cu-Zn binary systems were studied theoretically and experimentally. The concentration values at the physical phase boundaries of the interfaces simulated by the model and shown experimentally are related directly to the concentration values at the boundaries of the two-phase regions on the equilibrium binary phase diagrams. The numerical solution of the rate constants are greatly affected by these values along with the diffusion coefficient ratios. The propagation rate constant values were used to determine the concentration profile in each phase as well as the interfaces' locations. The predicted concentrations in all phases of the Ni-Zn and Cu-Zn binary systems agree well with those observed in the experimental investigations.

1 CHAPTER 1: INTRODUCTION

1.1 Thermal Energy Storage Technology

Recently, the strong need for novel energy alternatives has been a critical issue in most of social and industrial communities. In particular, earth planet is revealing to a catastrophic distortion everyday caused by using unsafe energy sources. These huge motivations led researchers to seek alternative energy sources which are safe, environmental friend, and relatively less cost. Solar energy has been considered as one of the safest energy sources; its availability, reliability and industry affordability made it a very attractive choice for many researchers in this field. Further, this kind of energy source is used in many engineering fields. Especially, space heating and electricity generation.

Nowadays, many of solar power plants are searching for an energy storage technology. In some of these plants, collector fields have been built to collect solar thermal energy. However, a lot of them do not have storage system that can be used to accumulate the collected energy for later use. The Leader for Thermal Energy Storage at the National Renewable Energy Laboratory (NREL), Greg Glatzmaier, clearly stated that the thermal energy storage is an attractive technology with the aim of reducing the overall cost [1]. This technology will assist exploiting the collected energy during the day time and store it for further use in the night time. For our study, this is was the start point of thinking about a Phase Change Material (PCM) that are sensitive to heat at elevated temperature by changing its status from liquid to solid and vice versa under heat control.

1.2 Phase Change Materials, PCMs

First, let's define the concept of PCMs. PCMs are simply substances that can store and release thermal energy by heating and cooling at sensible temperature. The mechanism of how an encapsulated phase change material alters its state from solid to liquid and vice versa can be shown in Figure (1). As shown in this Figure, after heating to a sensitive temperature, PCM changes its status from solid to liquid. Due to that, it absorbs the energy and holds it as storage. As the material cools down, it releases the energy to the surrounding and starts to solidify. An obvious simple example for this kind of materials is water/ice. PCMs have been successfully engaged in many applications such as heat exchangers, medical applications, air-conditioning, computer cooling systems and satellites thermal storage applications**.** In general, PCMs can be classified to two major groups: organic and inorganic compounds [2]. A comparison between these groups showing the advantages and disadvantages is illustrated in Table (1).

Table 1. Advantages and disadvantages of organic and inorganic PCMs [2].

Features	Organic PCMs	Inorganic PCMs
Corrosion	Non-corrosive	Corrosive to most metals
Stability	Chemically stable, no sub-cooling	Chemically unstable, suffering from decomposition and sub-cooling
Latent heat	High	High
Thermal conductivity	Low	High
Flammability	High	Non-flammable
Cost	Relatively high	Low

As a thermal storage option, phase change materials are promising candidates to play major rule in the energy industry. In power plant applications, the temperature enter the turbine is around 400 to 450C. We are looking for a material which possesses melting temperature in this range and has high latent heat of fusion. The selection is laid on Zn. Zn has a high melting temperature (419.5^0C) with a latent heat of fusion (100.9 kJ/kg). These two main characteristics make the zinc a promise option for our application. The zinc ingot has to be encapsulated within a metal with a high melting point much more than Zn such as Ni or Cu. The melting point of Ni and Cu are 1455.0°C and 1084.87°C according to their equilibrium phase diagrams. As a simulation for the thermal energy storage technique, the encapsulated zinc is heated up to 450^0C for designated exposure; and then it cools down to room temperature. Apparently, the investigation results ensured forming new solid layers at the Ni-Zn and Cu-Zn interfaces as a result of a diffusion process.

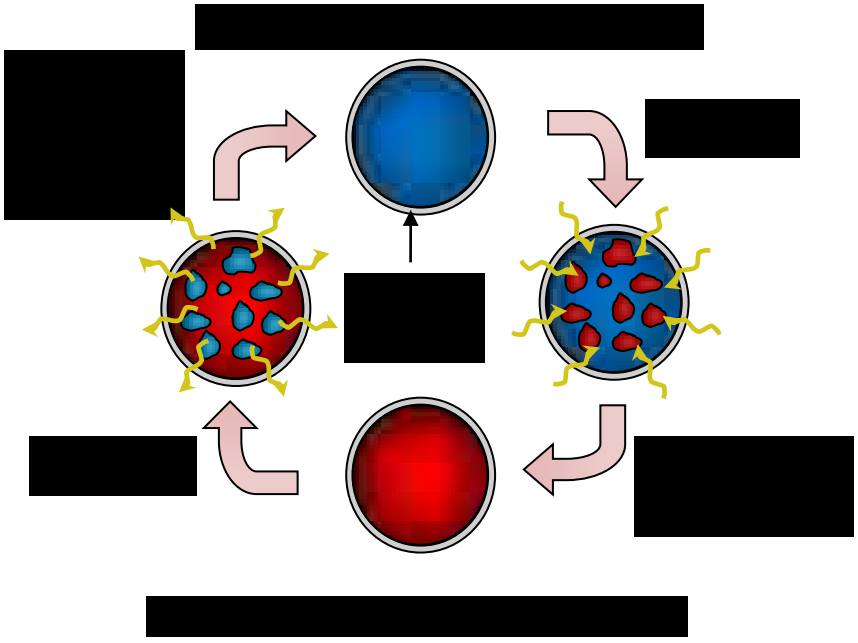

Figure 1. Phase change mechanism of a PCM [3].

1.3 Literature Review

Diffusion in binary systems has been investigated experimentally in many earlier studies [4-35]. In such experiments, a diffusion couple of two elements was exposed to heat for designated times and temperatures. During this process, distinct new phase layers are formed at the interface and grown with increasing the exposure time. Previously, many investigators have reported that some of these phases may not be distinguished from each other even with sufficient exposure time [4-9, 36-43]. In another study, phase formation in the Ni-Zn binary system had been studied at an annealing temperature of 400 ℃ [44]. In these investigations, layers formation was observed and the study was focused on phase identification for the formed layers and measuring individual layer thickness at two different annealing times. Castleman and Seigle [36, 37] asserted that distinguishable phases can be achieved by exposing the diffusion couple to sufficiently high temperatures and long times based on the alloy system being examined.

A solid-solid diffusion kinetics of a hypothetical binary system consisting of an inter-metallic compound layer, β, and two primary solid phases, α and γ had been analyzed theoretically [18]. For this binary system, a unidirectional semi-infinite diffusion mechanism is assumed. The diffusional direction is perpendicular to a flat interface and the diffusion process is controlled by the β inter-metallic compound layer diffusion coefficient, D^{β}. The inter-metallic compound layer is bound by two migration interfaces. The locations of the migration interfaces are proportional to the exposure time t, by the relationship, $z = K\sqrt{4D^{\beta}\, t}$; where K is the migration rate constant. For such a problem statement, an analytical solution was found for a solid-solid diffusion couple. A system of two coupled discontinuity equations is stated relating the constant

concentration boundary values and the migration rate constants. The hypothetical model was applied to Al-Fe binary system in a recent study [45]. In this study, the model result was directly compared to the parabolic law. However, the system of the discontinuity equations has not been solved for the migration rate constants K.

In the present work, diffusion in Ni-Zn and Cu-Zn binary systems has been investigated experimentally and analytically. For the Ni-Zn case study, the diffusion couple has been exposed to elevated temperature $(450\,℃)$ for designated exposure times, (1 hour, 2 hours, 4 hours, 8 hours and 16 hours). On the other hand, one sample of the Cu-Zn system has been exposed to similar condition for 8 hours. In such an elevated temperature, (high enough to reach melting point of one element of the diffusion couple), the rate of diffusion process is dominated by liquid phase diffusion coefficient. Multilayer of different phases is formed between the solid Ni/Cu and the liquid Zn. Based on the observation from the compositional analysis, several discontinuities prove many previous observations of multiple phase formation.

Referring to the phase diagram of Ni-Zn binary system at $450\,℃$ shown in Figure (11), four phases of α, β_1, γ and δ are clearly formed between the solid and liquid phases. Likewise, four phases of α, β', γ and ε are formed at the same temperature for the Cu-Zn binary system as shown in Figure (21). Our optical microscopic images do not show α and β' solid phases adjacent to the Ni or Cu elements, this is may be due to the fact that these phases grew very slowly and layer thickness of these layers are too small to be observed. Each two neighboring phases are distinct by two moving flat interfaces. It is considered that the original flat interface between Ni/Cu and Zn is the reference measurement point of the layer growth. It is also considered that the layers are growing in

a positive sense direction and therefore the propagation rate constants will follow the same manner.

The mathematical analysis is done using self-similar technique and it is generic for multilayer system. The analysis shows a consistent result for the concentration profiles with the experimental data. In addition, it also shows a good prediction for the experimental measurements of the phase's thicknesses and diffusion coefficient for each phase can be approximately obtained for the desired system.

1.4 Diffusion Mechanism and Phases Formation

Generally, diffusion can be defined as a natural transfer process of a substance into its surrounding region. The substance molecules transfer from higher concentration region to lower concentration region to achieve an equilibrium state by distributing the substance molecules throughout the system.

In our case, the diffusion couple is exposed to heat for different exposure times. One of the diffusion couple has lower melting point than the other one resulting in phase change for the lower melting point substance from solid to liquid while the high melting point substance remains in the solid state. As a result of concentration variation between the two substances at the interface, the higher concentration substance diffuse to the lower concentration in which layers of a new chemical composition phases will form at the interface. Referring to Ni-Zn binary phase diagram, at an elevated temperature, multiple phase will form between solid Ni and liquid Zn. Between each two adjacent phases, a transition region represents the interface discontinuity. Remarkably, Ni-Zn interface behaves as a flat interface which moves toward the solid region. Previously,

identical behavior was detected in the Cu-Al diffusion couple study [34]. As far as the interface moves, the layers will expand with time. From the mathematical modeling point of view, this kind of interface behavior makes the diffusion problem a moving boundary problem that should be treated carefully.

1.5 Self-Similar Technique

Previously, the similarity solutions were recognized through physical and dimensional procedures. It has been widely used in many mechanical applications such as fluid mechanics and heat transfer. For examples, extensive used of this type of solution in the boundary layer and convective heat diffusion problems. Recently, similarity technique was proposed to build up a large time approximate solutions of partial differential equations based on a balancing argument [46]. A universal parameter was introduced to reduce the partial differential equation to another much easier partial differential equation function of one independent variable.

The assumption here is the migration of the interface has the same shape (similar) with the time progresses. Additionally, the diffusion media is unbounded, and therefore has no characteristic length. Thus we can employ what is termed similarity solution. This technique is to introduce a stretching variable that depend on space and time and employ it into the original equations after some necessary transformations. Particularly, the original partial differential mass diffusion equation can be reduced to an ordinary differential equation which is much easier to handle analytically than the original equation.

2 CHAPTER 2: THEORETICAL APPROACH

According to a typical multiple phase binary system, as a result of diffusion process between two pure elements, stable phases are formed at the diffusion couple interface. These phases are separated by transition equilibrium regions which represent the concentration jump between each of the two adjacent phases. If the diffusion couple is exposed to an elevated temperature (high enough to reach a stable liquid phase of the low melting point element) for a sufficient time, a solid-liquid diffusion mechanism can be considered. Physically, these phases are appearing to grow with increasing exposure time concurrently in a solid-liquid diffusion media. The original interface is moving towards the solid phase [33]. However, comparing with other moving interfaces, its movement is extremely slow. Based on this fact, it can be assumed that the new interfaces are propagating in one direction in a positive sense with much higher propagation rate than the original solid-solid front. Consequently, the reference point of measurements is the original interface of the solid phase. Also, it can be assumed that the diffusion is semi-infinite into the liquid phase but finite in the intermediate phases. The diffusion coefficients are assumed to be independent of concentration.

2.1 Governing Equations

The diffusion phenomenon is described by Fick's law: $J_p = -D_p \nabla C_p$, where C_p denotes the concentration of phase p, D_p is the diffusion coefficient of phase p and J_p is the diffusive flux of phase p. The concentration of mass of phase p can then be written as,

$$\frac{\partial C_p}{\partial t} = D_p \frac{d^2 C_p}{dx^2} \qquad (p = i, j, k, \dots \dots etc) \qquad (1)$$

$C_p(x,t)$ is considered as a function of time t and distance x. A schematic drawing for the concentration profile of a multiple phase binary system is shown in Figure 2. In this Figure, the ordinate shows the concentration of the diffused element, C_p and the abscissa indicates the distance, x measured from the original interface. The solid lines represent the predicted concentration profile in each layer and the dashed lines indicate the interfaces. The indices$(i, j, k, \ldots \ldots etc)$ represent the formed phases between solid and liquid phases. Between two neighboring phases, for example (j, k), φ_{jk} is the location of the propagation front. For such an interface, c_{jk} and c_{kj} are the concentration values associated with this interface. The jumps in concentration and the values of concentration at the boundaries are directly tied to the phase diagrams of multiple phase systems.

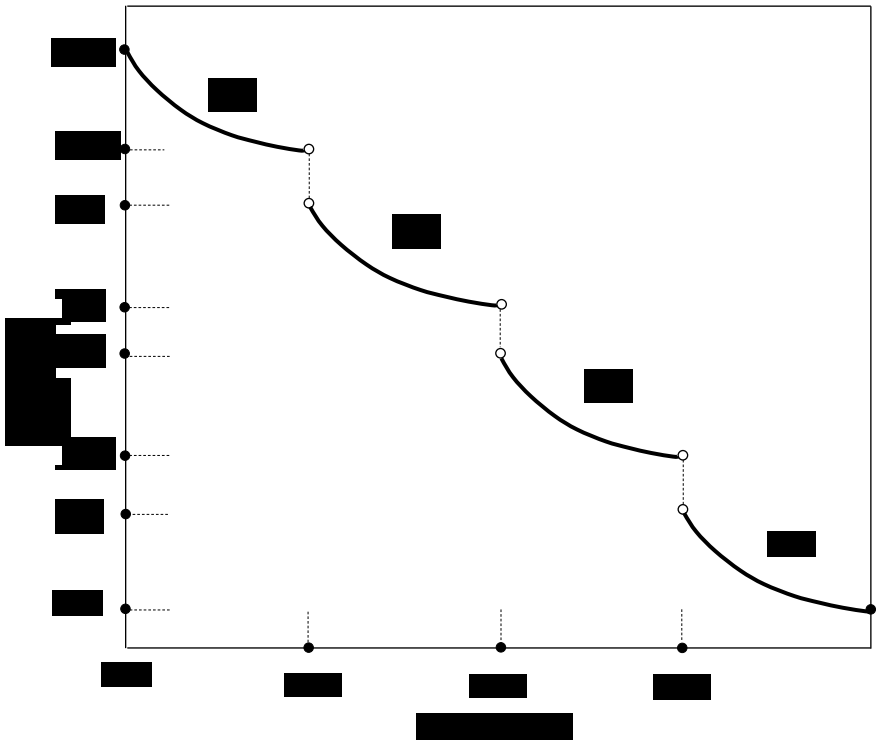

Figure 2. A schematic drawing for the concentration profile of a multiple phase binary system

The interface discontinuity is defined by the relationship between the flux balance and the migration rate of the interface [47, 48]. With,

$$c_{jk} = \lim_{x \to \varphi_{jk}^{-}} C_j \tag{2a}$$

And

$$c_{kj} = \lim_{x \to \varphi_{jk}^{+}} C_k \tag{2b}$$

The mass concentration at the interface φ_{jk} yields,

$$\left(c_{jk} - c_{kj}\right) \frac{\partial \varphi_{jk}}{\partial t} = -D_j \left.\frac{dC_j}{dx}\right|_{\varphi_{jk}^{-}} + D_k \left.\frac{dC_k}{dx}\right|_{\varphi_{jk}^{+}} \tag{3}$$

The plus and minus signs refer that the interface approaching from to the right and left, respectively.

The other boundary conditions imposed on C_j are,

$$\lim_{x \to \varphi_{ij}^{+}} C_j\left(\varphi_{ij}^{+}, t\right) = c_{ji}\,, \tag{4a}$$

$$\lim_{x \to \varphi_{jk}^{-}} C_j\left(\varphi_{jk}^{-}, t\right) = c_{jk} \tag{4b}$$

2.2 Self-Similar Solution

2.2.1 Similarity Variable Establishment

In the present solution technique, the total layer thickness is assumed to retain its same shape when it is scaled on η. Here η is defined as the similarity variable, which is dependent on x and t and has the form,

$$\eta = a\, x^b t^k \tag{5}$$

where a, b and k are all constants. The main idea is to reduce the partial differential diffusion equation (1) to an ordinary differential equation function of η only. The next step is to find the values of a, b and k that make the resultant equation solvable. Starting with the time derivative term in the diffusion equation (1), we have,

$$\frac{\partial c}{\partial t} = \frac{\partial c}{\partial \eta}\frac{\partial \eta}{\partial t} = c' \frac{\partial \eta}{\partial t} = c' a\, x^b k\, t^{k-1} = c'(a\, x^b\, t^k)\frac{k}{t} = c'\eta\frac{k}{t} \tag{6}$$

The right hand side will be transformed as follow,

$$D\frac{d^2c}{dx^2} = D\frac{\partial}{\partial x}\left(\frac{\partial c}{\partial \eta}\frac{\partial \eta}{\partial x}\right) = D\frac{\partial}{\partial \eta}\left(\frac{\partial \eta}{\partial x}\right)^2\left(\frac{\partial c}{\partial \eta}\right) = D\left(\frac{\partial \eta}{\partial x}\right)^2\left(\frac{d^2c}{d\eta^2}\right) = D\,(a\, b\, x^{b-1}t^k)^2 c''$$

$$= c'' D\left(a\, x^b t^k \frac{b}{x}\right)^2 = c'' D\, \eta^2 \left(\frac{b}{x}\right)^2 \tag{7}$$

Equating both terms in equations (6) and (7) leads to,

$$c'\eta\frac{k}{t} = c'' D\, \eta^2 \left(\frac{b}{x}\right)^2$$

$$c'\,\frac{k}{t} = c''\, D\, \eta \left(\frac{b}{x}\right)^2$$

$$c'' - c'\frac{kx^2}{t\, Db^2\eta} = 0 \tag{8}$$

The ordinary differential equation of the form ($c'' + 2\eta c' = 0$) is solvable. We need to seek this form of equation by setting $\frac{kx^2}{t\, Db^2\eta} = -2\eta$. As a result, we will have,

$$\eta^2 = -\frac{kx^2}{2t\ Db^2} \tag{9}$$

Or by taking the square root of η in equation (9) and compare it with the equation (5), we get,

$$\eta = a\ x^b t^k = \left(-\frac{kx^2}{2t\ Db^2}\right)^{\frac{1}{2}} = \left(-\frac{k}{2\ D}\right)^{\frac{1}{2}} \frac{x}{b}\ t^{-\frac{1}{2}} \tag{10}$$

If we equate the constants in both sides of equation (10), we can deduce $k = -\frac{1}{2}$, $b = 1$ and $a = \sqrt{\frac{1}{4D}}$, and subsequently,

$$\eta = \frac{x}{\sqrt{4Dt}} \tag{11}$$

Equation (11) represents Boltzmann transformation formula.

2.2.2 Analytical Solution

Equations (1-4) pose a self-similar solution. The Boltzmann transformation formula can be used as a similarity variable to reduce the partial differential diffusion equation to an ordinary differential equation,

$$\eta = \frac{x}{\sqrt{4D_L\ t}} \tag{12}$$

Where η, is the growth rate and $D_L$is the liquid phase diffusion coefficient. The location of the interfaces, $x = \varphi_{ij}$ can be expressed in terms of similarity variable as,

$$\eta_{ij} = \frac{\varphi_{ij}}{\sqrt{4D_L\ t}} \tag{13}$$

Equation (1) is reduced to,

$$\frac{d^2C_p}{d\eta^2} + 2\Delta_p\eta \ \frac{\partial C_p}{\partial \eta} = 0 \qquad\qquad (p = i, j, k, \dots \dots etc) \tag{14}$$

Where $\Delta_p = D_L/D_p$ is defined as the diffusion coefficients ratio.

The appropriate boundary conditions for each phase is written as,

$$C_j\left(\eta_{ij}^{+}\right) = c_{ji}\,, \tag{15a}$$

$$C_j\left(\eta_{jk}^{-}\right) = c_{jk} \tag{15b}$$

Equation (3) can be transformed as well. The migration rate term can be written as,

$$\frac{\partial \varphi_{jk}}{\partial t} = \eta_{jk}\frac{1}{2}\sqrt{\frac{4D_L}{t}} + \frac{\partial \eta_{jk}}{\partial t}\sqrt{4D_L\, t} = \eta_{jk}\frac{1}{2}\sqrt{\frac{4D_L}{t}} + \frac{\partial \eta_{jk}}{\partial \eta}\frac{\partial \eta}{\partial t}\sqrt{4D_L\, t}$$

$$\frac{\partial \varphi_{jk}}{\partial t} = \eta_{jk}\frac{1}{2}\sqrt{\frac{4D_L}{t}} - \frac{\eta_{jk}}{2t}\sqrt{4D_L\, t}\ \frac{\partial \eta_{jk}}{\partial \eta}$$

And therefore,

$$\frac{\partial \varphi_{jk}}{\partial t} \ = \sqrt{\frac{D_L}{t}}\left(\eta_{jk} - \eta_{jk}\ \frac{\partial \eta_{jk}}{\partial \eta}\right) \tag{16}$$

Also, concentration gradient terms can be easily transformed as follow,

$$\left.\frac{dC_j}{dx}\right|_{\varphi_{jk}^{-}} = \frac{1}{\sqrt{4D_L\, t}}\left.\frac{dC_j}{d\eta}\right|_{\eta_{jk}^{-}} \tag{17a}$$

$$\left.\frac{dC_k}{dx}\right|_{\varphi_{jk}^{+}} = \frac{1}{\sqrt{4D_L t}} \left.\frac{dC_k}{d\eta}\right|_{\eta_{jk}^{+}} \tag{17b}$$

Reconstruct equation (3) using equations (16) and (17) gives,

$$\left(c_{jk} - c_{kj}\right)\sqrt{\frac{D_L}{t}}\left(\eta_{jk} - \eta_{jk}\,\frac{\partial \eta_{jk}}{\partial \eta}\right) = -D_j \frac{1}{\sqrt{4D_L\, t}} \left.\frac{dC_j}{d\eta}\right|_{\eta_{jk}^{-}} + D_k \frac{1}{\sqrt{4D_L t}} \left.\frac{dC_k}{d\eta}\right|_{\eta_{jk}^{+}} \tag{18}$$

Simplifying this equation leads to,

$$2\left(\eta_{jk} - \eta_{jk}\,\frac{\partial \eta_{jk}}{\partial \eta}\right)\left(c_{jk} - c_{kj}\right) = \frac{1}{\Delta_k}\, C_k'\left(\eta_{jk}^{+}\right) - \frac{1}{\Delta_j} C_j'\left(\eta_{jk}^{-}\right) \tag{19}$$

The ordinary differential equation (14) can be written as,

$$C_p'' + 2\Delta_p \eta\, C_p' = 0 \tag{20}$$

Dividing both sides of equation (20) by C_p', we can write,

$$\frac{C_p''}{C_p'} = -2\Delta_p \eta \tag{21}$$

The integration of equation (21) leads to,

$$\ln C_p' = -\Delta_p \eta^2 + E \tag{22}$$

Where E is a constant. Taking the exponential for both sides yields,

$$C_p'(\eta) = F_p\, \exp\left(-\Delta_p \eta^2\right) \tag{23}$$

Where $F_p = \exp(E) =$ constant.

For phase j, equation (23) can be written as,

$$C_j'(\eta) = F_j \exp\left(-\Delta_j \eta^2\right) \tag{24}$$

Taking the integration leads to,

$$C_j(\eta)\Big|_{\eta_{ij}^+}^{\eta_{jk}^-} = F_j \int_{\eta_{ij}^+}^{\eta_{jk}^-} \exp(-\Delta_j \eta^2)\, d\eta \tag{25}$$

Evaluating the integration and applying the appropriate boundary conditions yields,

$$C_j\left(\eta_{jk}^-\right) - C_j\left(\eta_{ij}^+\right) = -F_j \left\{\frac{\sqrt{\pi}}{2\sqrt{\Delta_j}} \left[erf\left(\sqrt{\Delta_j}\eta_{ij}^+\right) - erf\left(\sqrt{\Delta_j}\eta_{jk}^-\right)\right]\right\} \tag{26}$$

And therefore,

$$F_j = -\frac{2\sqrt{\Delta_j}\left(c_{jk} - c_{ji}\right)}{\sqrt{\pi}\left(erf\left(\sqrt{\Delta_j}\eta_{ij}\right) - erf\left(\sqrt{\Delta_j}\eta_{jk}\right)\right)} \tag{27}$$

Substituting the value of F_j into equation (24) and replace η with η_{jk}^- give an expression for $C_j'\left(\eta_{jk}^-\right)$ as follow,

$$C_j'\left(\eta_{jk}^-\right) = -\frac{2\sqrt{\Delta_j}\left(c_{jk} - c_{ji}\right)}{\sqrt{\pi}\left(erf\left(\sqrt{\Delta_j}\eta_{ij}\right) - erf\left(\sqrt{\Delta_j}\eta_{jk}\right)\right)}\, exp\left(-\Delta_j {\eta_{jk}}^2\right) \tag{28}$$

Likewise, for phase k, equation (23) can be written as,

$$C_k'(\eta) = F_k \exp(-\Delta_k \eta^2) \tag{29}$$

Taking the integration leads to,

$$C_k(\eta)|_{\eta_{jk}^+}^{\eta_{kl}^-} = F_k \int_{\eta_{jk}^+}^{\eta_{kl}^-} \exp(-\Delta_k \eta^2)\, d\eta \tag{30}$$

Evaluating the integration and applying the appropriate boundary conditions yields,

$$C_k(\eta_{kl}^-) - C_k(\eta_{jk}^+) = -F_k \left\{ \frac{\sqrt{\pi}}{2\sqrt{\Delta_k}} \left[erf\left(\sqrt{\Delta_k}\eta_{jk}^+\right) - erf\left(\sqrt{\Delta_k}\eta_{kl}^-\right) \right] \right\} \tag{31}$$

And therefore,

$$F_k = -\frac{2\sqrt{\Delta_k}(c_{kl} - c_{kj})}{\sqrt{\pi}\left(erf\left(\sqrt{\Delta_k}\eta_{jk}\right) - erf\left(\sqrt{\Delta_k}\eta_{kl}\right) \right)} \tag{32}$$

Substituting the value of F_k into equation (24) and replace η with η_{jk}^+ give an expression for $C_k'(\eta_{jk}^+)$ as follow,

$$C_k'(\eta_{jk}^+) = -\frac{2\sqrt{\Delta_k}(c_{kl} - c_{kj})}{\sqrt{\pi}\left(erf\left(\sqrt{\Delta_k}\eta_{jk}\right) - erf\left(\sqrt{\Delta_k}\eta_{kl}\right) \right)}\, exp\left(-\Delta_k {\eta_{jk}}^2\right) \tag{33}$$

Obviously, since the values of the concentration at the boundaries are constant, it is necessary that the value of the propagation rate is constant too. Therefore, η_{jk} is independent on η. So we can write,

$$\frac{\partial \eta_{jk}}{\partial \eta} = 0 \tag{34}$$

Then, equation (19) becomes,

$$2\,\eta_{jk}\left(c_{jk} - c_{kj}\right) = \frac{1}{\Delta_k}\, C_k'(\eta_{jk}^+) - \frac{1}{\Delta_j} C_j'(\eta_{jk}^-) \tag{35}$$

The substitution of equations (28) and (33) into equation (35) gives,

$$\left(c_{jk}-c_{kj}\right)=-\frac{\left(c_{kl}-c_{kj}\right)}{\eta_{jk}\sqrt{\pi\,\Delta_k}\left(erf\left(\sqrt{\Delta_k}\eta_{jk}\right)-erf\left(\sqrt{\Delta_k}\eta_{kl}\right)\right)}\,exp\left(-\Delta_k{\eta_{jk}}^2\right)$$

$$+\frac{\left(c_{jk}-c_{ji}\right)}{\eta_{jk}\sqrt{\pi\,\Delta_j}\left(erf\left(\sqrt{\Delta_j}\eta_{ij}\right)-erf\left(\sqrt{\Delta_j}\eta_{jk}\right)\right)}\,exp\left(-\Delta_j{\eta_{jk}}^2\right) \tag{36}$$

System of equations similar to equation (36) can be generated if multiple phase type of problem is addressed.

The concentration profile can be found for each phase by integrating the concentration gradient. For instance, the concentration profile of phase *j* denoted by $C_j(\eta)$ can be obtained by integrating equation (24) indefinitely as follow,

$$C_j(\eta)=\ F_j\int\exp\left(-\Delta_j\eta^2\right)d\eta+G \tag{37}$$

Or we can write,

$$C_j(\eta)=F_j\frac{\sqrt{\pi}}{2\sqrt{\Delta_j}}\,erf\left(\sqrt{\Delta_j}\eta\right)+G \tag{38}$$

Using equation (28) for the value of F_j and applying the boundary condition (16a),

$$C_j\left(\eta_{ij}^{+}\right)=-\frac{2\sqrt{\Delta_j}\left(c_{jk}-c_{ji}\right)}{\sqrt{\pi}\left(erf\left(\sqrt{\Delta_j}\eta_{ij}\right)-erf\left(\sqrt{\Delta_j}\eta_{jk}\right)\right)}\frac{\sqrt{\pi}}{2\sqrt{\Delta_j}}\,erf\left(\sqrt{\Delta_j}\eta_{ij}^{+}\right)+G \tag{39}$$

Or we can write,

$$G=c_{ji}\ +\frac{\left(c_{jk}-c_{ji}\right)}{\left(erf\left(\sqrt{\Delta_j}\eta_{ij}\right)-erf\left(\sqrt{\Delta_j}\eta_{jk}\right)\right)}\,erf\left(\sqrt{\Delta_j}\eta_{ij}^{+}\right) \tag{40}$$

Now, by substituting the values of the constants G and F_j into equation (38), it gives,

$$C_j(\eta) = c_{ji} - \frac{2\sqrt{\Delta_j}(c_{jk} - c_{ji})}{\sqrt{\pi}\left(erf\left(\sqrt{\Delta_j}\eta_{ij}\right) - erf\left(\sqrt{\Delta_j}\eta_{jk}\right)\right)} \frac{\sqrt{\pi}}{2\sqrt{\Delta_j}}\, erf\left(\sqrt{\Delta_j}\eta\right)$$

$$+ \frac{(c_{jk} - c_{ji})}{\left(erf\left(\sqrt{\Delta_j}\eta_{ij}\right) - erf\left(\sqrt{\Delta_j}\eta_{jk}\right)\right)}\, erf\left(\sqrt{\Delta_j}\eta_{ij}\right) \tag{41}$$

Or we can write

$$C_j(\eta) = c_{ji} + \frac{(c_{jk} - c_{ji})\left(erf\left(\sqrt{\Delta_j}\eta\right) - erf\left(\sqrt{\Delta_j}\eta_{ij}\right)\right)}{erf\left(\sqrt{\Delta_j}\eta_{jk}\right) - erf\left(\sqrt{\Delta_j}\eta_{ij}\right)} \tag{42}$$

Equation (42) represents the concentration profile of phase *j* as a function of the similarity variable η. Using the definitions of the similarity variable η and the propagation rate constants, equation (43) can be written in terms of distance x, and time t, as follow,

$$C_j(x,t) = c_{ji} + \frac{(c_{jk} - c_{ji})\left(erf\left(\sqrt{\Delta_j}\frac{x}{\sqrt{4D_L t}}\right) - erf\left(\sqrt{\Delta_j}\frac{\varphi_{ij}}{\sqrt{4D_L t}}\right)\right)}{erf\left(\sqrt{\Delta_j}\frac{\varphi_{jk}}{\sqrt{4D_L t}}\right) - erf\left(\sqrt{\Delta_j}\frac{\varphi_{ij}}{\sqrt{4D_L t}}\right)} \tag{43}$$

2.3 Numerical Method

A system of equations similar to equation (36) can be generated if a multiple phases separated by multiple propagation front are considered. Equation (36) is a nonlinear algebraic equation function of the growth constant η_{jk}. Similar equation will be derived for each propagation front when multiple phases are present. Such systems of

nonlinear equations are solved numerically using *Maple ™ 15*. More details in the numerical solution and *Maple ™ 15* code can be found in appendix A. The values of η_{jk} can then be used to obtain the concentration profiles of phase j using equation (42).

3 CHAPTER 3: EXPERIMENTAL PROCEDURE

Commercially pure nickel (Ni alloy 200) and 99.997% pure zinc were used in this investigation. Five 41 mm-long rods were sectioned from 12.7 mm diameter nickel bar stock. Holes were drilled perpendicular to the central axis at one end of each bar so that each rod could be suspended in molten zinc by a small diameter stainless steel rod. The surfaces of the nickel rods were then prepared with 600 grit SiC abrasive paper to remove surface imperfections and contaminants. The rods were then cleaned in a degreasing agent and rinsed in alcohol. Individual crucibles, containing 98.2 grams of zinc, were heated to 450^0C until molten. Once molten, a nickel rod was suspended in the zinc for an allotted amount of time. The designated times were 1 hour, 2 hours, 4 hours, 8 hours, and 16 hours. After exposure to the molten zinc, the rods were quickly removed and quenched in water in order to retain the microstructure at the elevated temperature. The rods were then sectioned into thin discs and metallographically prepared to a 0.05 micron finish. Light optical microscopy was then used to visually inspect the extent of the intermediate phase formation, as well as determine the thickness of the phase layers with respect to the exposure time for each specimen. The same procedure was used for a copper/zinc specimen; however, it was only exposed to the molten zinc for 8 hours at 450^0C. The copper was commercially pure (Cu alloy 101).A Hitachi 4300 Scanning Electron Microscope was then used to generate phase identification of each layer. The working voltage was 5 kV. Wavelength dispersive spectroscopy analysis of the multiple phase layers provided compositional differences between each layer. The compositional data was used to verify model results.

4 CHAPTER 4: OPTICAL MICROSCOPY

Light optical photomicrographs of the Ni-Zn system at different exposure times are shown in Figures (3), (4), (5), (6) and (7). As well, a light optical photomicrograph for the Cu-Zn system at 8 hour exposure times is shown in Figure (8). Between the regions of nickel and zinc and copper and zinc, there are distinct regions wherein intermediate phases formed. The intermediate phases show preferential growth in the radial direction, which is evident in the grain structure of the outermost layer in the Ni-Zn system. The Cu-Zn system also displays this preferential growth; however, it is not as evident. Clear boundaries within the intermediate phases are also observed. From this, it can be inferred that within each of the regions between the nickel and zinc and the copper and zinc that there are multiple changes in structure and composition.

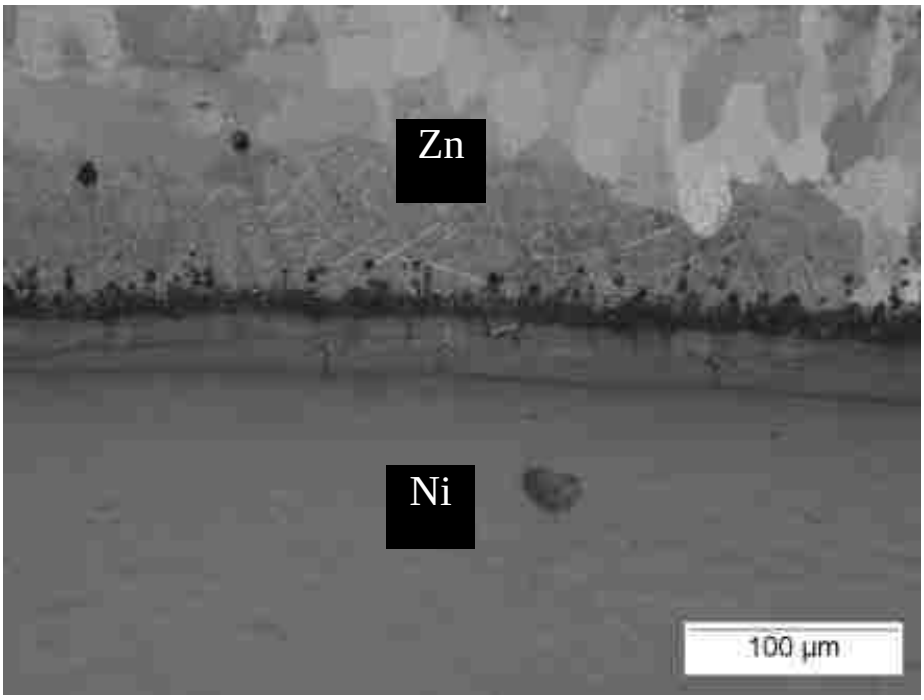

Figure 3. Light optical photomicrographs of the Ni-Zn system after 1 hour exposure

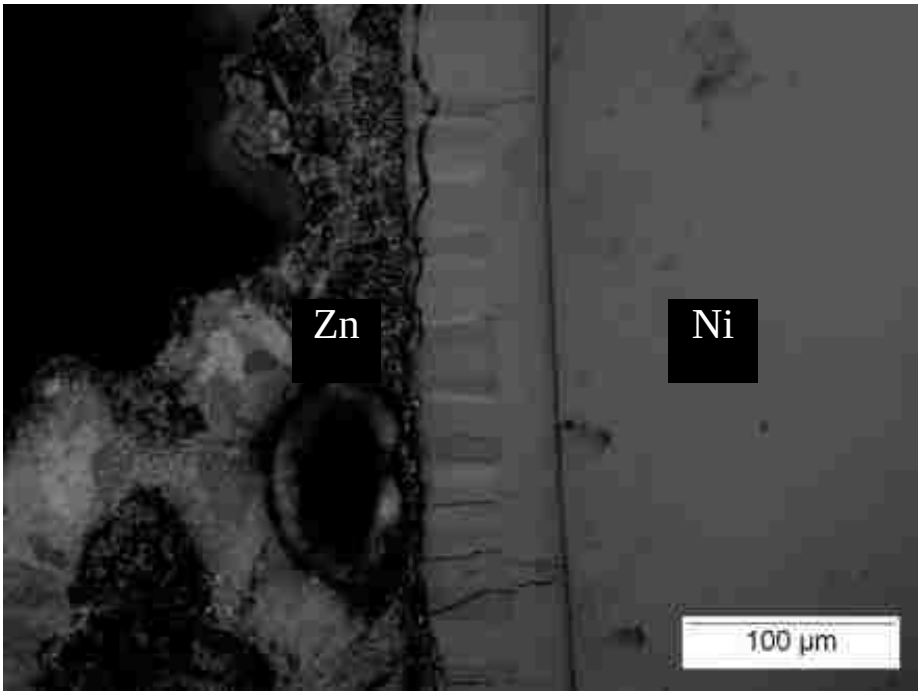

Figure 4. Light optical photomicrographs of the Ni-Zn system after 2 hours exposure.

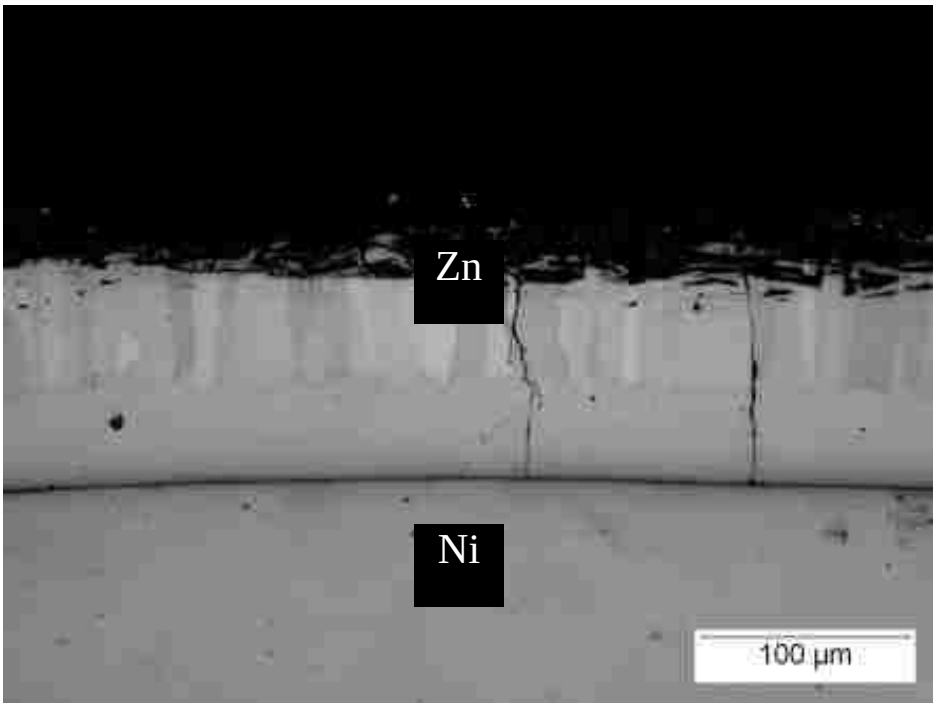

Figure 5. Light optical photomicrographs of the Ni-Zn system after 4 hours exposure.

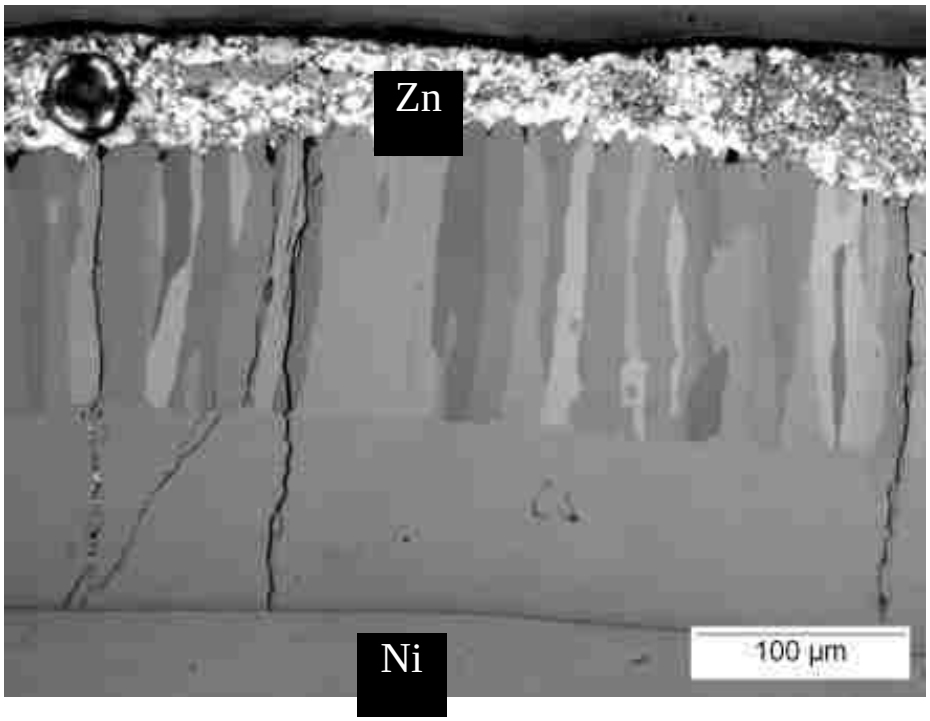

Figure 6. Light optical photomicrographs of the Ni-Zn system after 8 hours exposure.

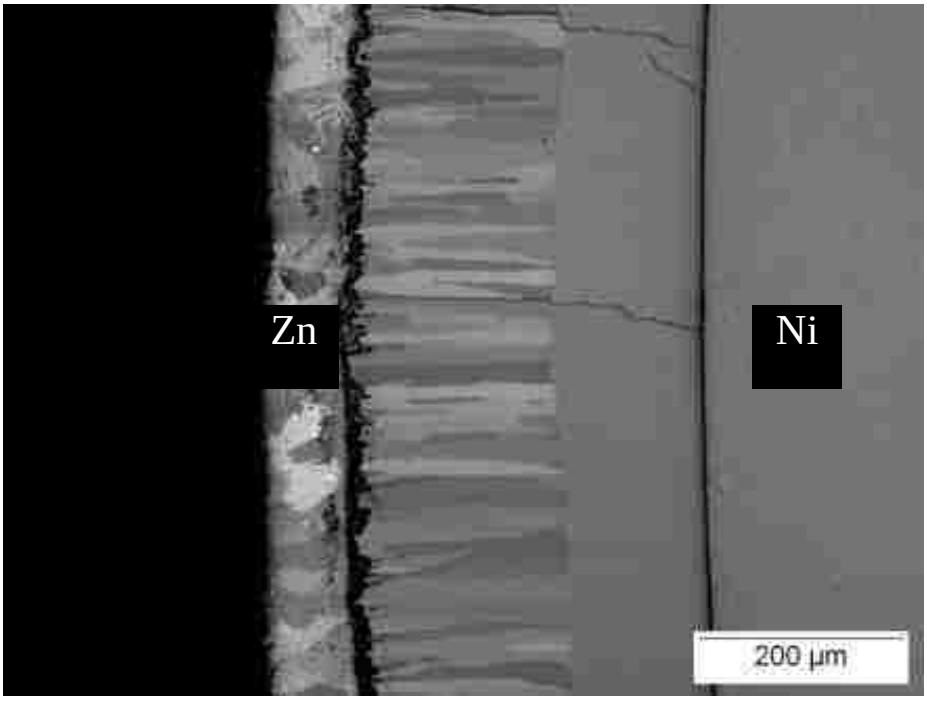

Figure 7. Light optical photomicrographs of the Ni-Zn system after 16 hours exposure.

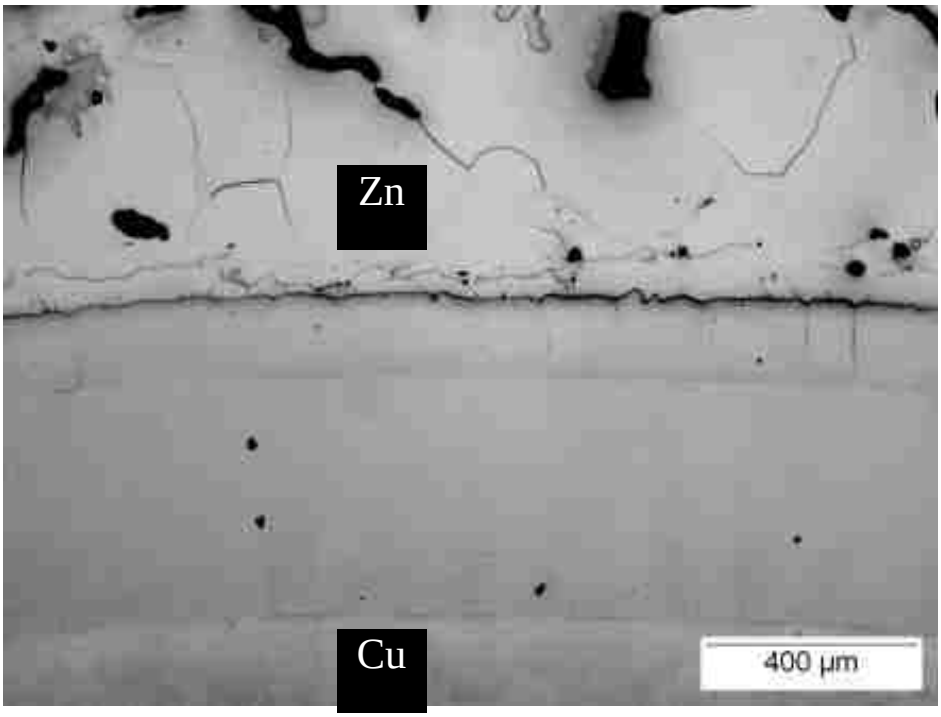

Figure 8. Light optical photomicrographs of the Cu-Zn system after 8 hour exposure.

According to the Ni-Zn and Cu-Zn equilibrium phase diagrams, there should be four intermediate phases present between the two pure materials. However, only two intermediate phases can be resolved from light optical inspection of both the Ni-Zn system the Cu-Zn system. The other phases may be present, but the thickness of the layers may be so small that they cannot be resolved by light optical techniques.

It can be seen in figures (3-8) that as the exposure time increases, the thickness of the intermediate phases also increases. This trend can be seen in the individual intermediate phases as well. The average values of the interfaces' locations $\varphi_{\delta L}$ and $\varphi_{\gamma\delta}$ at different exposure times for the Ni-Zn system are given in Table (2). With respect to the Cu-Zn system, the average values of the interface locations $\varphi_{\varepsilon L}$ for eight

hours exposure time is 616.4 microns whereas the average values of the interface locations $\varphi_{\gamma\varepsilon}$ is 460.4 microns.

Table 2. Average value of the interface locations $\varphi_{\delta L}$ and $\varphi_{\gamma\delta}$ at different exposure times for the Ni-Zn system.

Interface locations	**Exposure Time**				
	1hr	**2hr**	**4hr**	**8hr**	**16hr**
$\varphi_{\delta L}$ **(µm)**	26.4	70.8	115.8	227.2	335.8
$\varphi_{\gamma\delta}$ **(µm)**	12.8	29.6	45.4	95.4	142

5 CHAPTER 5: RESULTS AND DISCUSSION

5.1 Single Phase Model: Al-Zn Theoretical Case Study

The set of nonlinear algebraic equation for each interface separating phases should be used to calculate the interface location. For instance, the formation of three phases means that there will be two nonlinear equations for two interfaces separating three phases. From the Al-Zn phase diagram illustrated in Figure (9), a solid phase along with the liquid phase separated by a transition region, are considered a single phase problem with a single propagation front. A nonlinear equation is describing the relationship between the constant concentration values and the rate constant. According to Figure (9), the dotted red line indicates the temperature level at $450\,℃$. Along this line, concentration values are well indicated between each phase at the equilibrium lines. The vertical blue dashed lines indicate the concentration values on the abscissa.

According to equation (36), the indices i, j, k and l can be replaced by the phases notation Al, α, L and Zn, respectively. In addition, the constant concentration values at the boundaries can be written as ($c_{Al\,\alpha}, c_{\alpha L}, c_{L\alpha}$ and $c_{L\,Zn}$) and have the values (1.0, 0.33, 0.155 and 0), respectively. The values of Δ_α and Δ_L can be assumed depending on the proper fit to the experimental phase thickness data. For demonstration purposes of this case study, it is assumed that Δ_α and Δ_L have the values 1×10^2 and 1, respectively.

Equation (36), with the parameters related to this case is solved to determine the value of ($\eta_{\alpha L} = 0.03240495775$). This value will be different at different temperature since the concentrations at the boundaries will be different. Also, $\eta_{\alpha L}$ is dependent strongly on the value of Δ_α. The value of $\eta_{\alpha L}$ can be used to evaluate the concentration

profile of Al using equation (42) as shown in Figure (10). In this Figure, the ordinate shows the concentration of the Al and the abscissa indicates the dimensionless variable η. The dotted red line represents the phase α and the solid line indicates the concentration of Al in liquid Zn. The discontinuity is very clear at $\eta = \eta_{\alpha L}$.

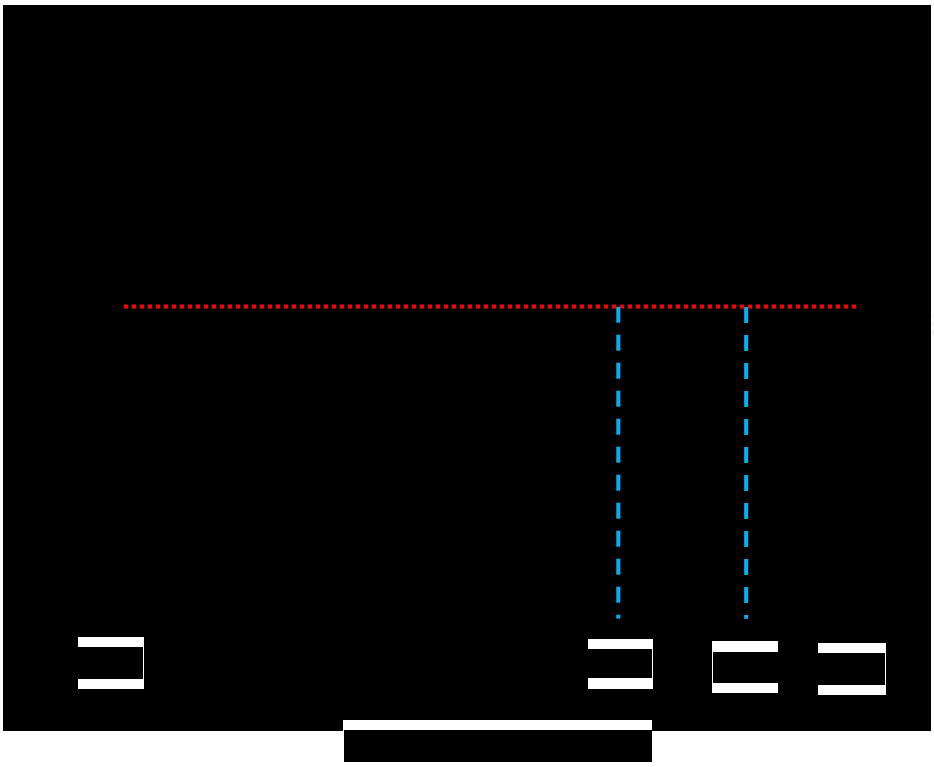

Figure 9. Al-Zn equilibrium phase diagram [49].

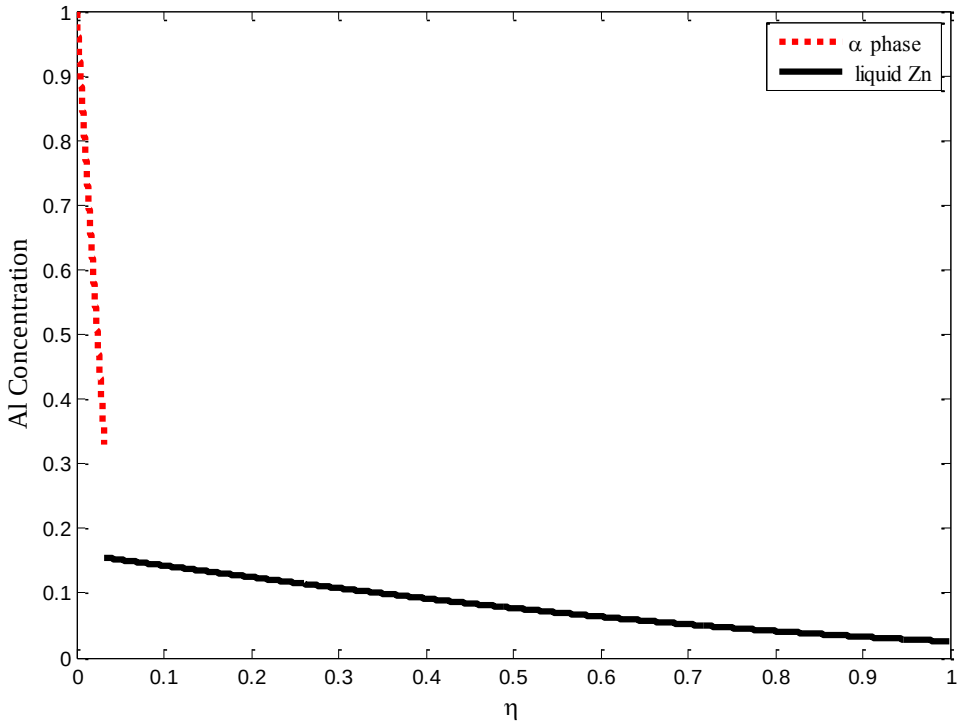

Figure 10. Concentration profile of the Al-Zn diffusion couple based on self-similar solution.

5.2 Multiple phase Model: Ni-Zn Binary System

A multiple phase model can be considered using Ni-Zn binary system. In such binary system as mentioned before, four phases α, β_1, γ and δ, at temperature 450 ℃ appear to be stable phases according to the Ni-Zn binary phase diagram illustrated in Figure (11). Referring to this Figure, a transition region between each of the two single phase's regions represents the propagation front.

A system of four nonlinear equations describes the relationship between the constant concentration values and the rate constants. These four equations presented in equation (36) with j and k of being α, β_1, γ and δ represents coupled nonlinear equations for $\eta_{\alpha\beta_1}, \eta_{\beta_1\gamma}, \eta_{\gamma\delta}$ and $\eta_{\delta L}$. According to Figure (11), the dotted red line represents the

temperature at 450 ℃. Clearly, along this line, the concentration at the four interfaces and boundaries are illustrated. The blue lines are drawn to indicate the values of the concentration on the abscissa.

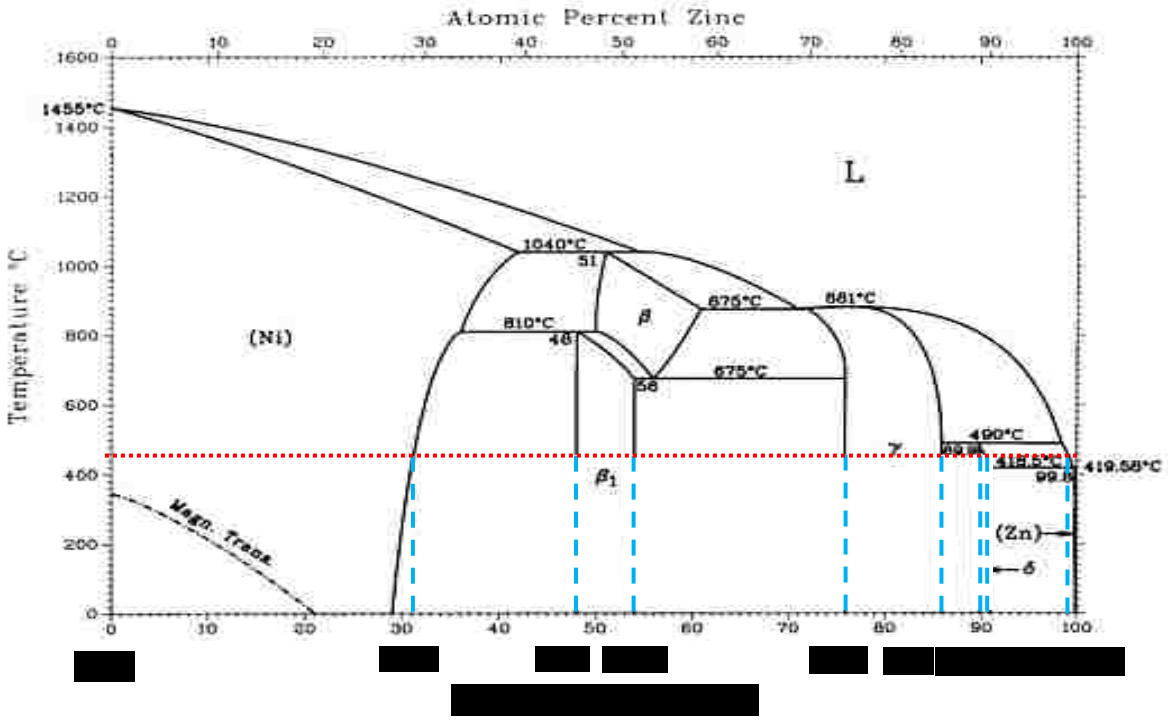

Figure 11. Ni-Zn equilibrium phase diagram [50].

At the first interface $\eta_{\alpha\beta_1}$ between phase α and phase β_1, the indices i, j, k and l in equation (36), represent Ni, α, β_1 and γ, respectively. The values of the concentration boundaries at this interface (c_{ij}, c_{jk}, c_{kj} and c_{jl}) represent ($c_{Ni\,\alpha}, c_{\alpha\beta_1}, c_{\beta_1\alpha}$ and $c_{\beta_1\gamma}$), respectively. At the interface $\eta_{\beta_1\gamma}$, between the β_1 phase and the γ phase, the indices i, j, k and l in equation (36) represent the phase notation α, β_1, γ and δ, respectively. The corresponding values of the concentration boundaries at this interface (c_{ij}, c_{jk}, c_{kj} and c_{jl}) represent ($c_{\alpha\beta_1}, c_{\beta_1\gamma}, c_{\gamma\beta_1}$ and $c_{\gamma\delta}$), respectively. At the interface $\eta_{\gamma\delta}$ between the γ

phase and the δ phase, the indices i, j, k and l in equation (36) represent the phases notation β_1, γ, δ and L, respectively. Therefore, the values of the concentration boundaries at this interface (c_{ij}, c_{jk}, c_{kj} and c_{jl}) represent ($c_{\beta_1\gamma}, c_{\gamma\delta}, c_{\delta\gamma}$, and $c_{\delta L}$), respectively. Lastly, at the solid-liquid interface $\eta_{\delta L}$, the indices i, j, k and l in equation (36), can be replaced by the phases notation γ, δ, L and Zn, respectively. Consequently, the values of the concentration boundaries at this interface (c_{ij}, c_{jk}, c_{kj} and c_{jl}) represent ($c_{\gamma\delta}$, $c_{\delta L}, c_{L\delta}$, and $c_{L\,zn}$), respectively. According to Figure (11), the values of ($c_{Ni\,\alpha}, c_{\alpha\beta_1}, c_{\beta_1\alpha}, c_{\beta_1\gamma}, c_{\gamma\beta_1}, c_{\gamma\delta}$, $c_{\delta\gamma}$, $c_{\delta L}, c_{L\delta}$ and $c_{L\,zn}$) are about (1.0, 0.68, 0.52, 0.47, 0.24, 0.14, 0.10, 0.09, 0.015 and 0). The values of the diffusion coefficients ratios, $\Delta_\alpha, \Delta_{\beta_1}, \Delta_\gamma, \Delta_\delta$ and Δ_L are selected to fit best to the experimentally measured phase thickness data. For instance, higher diffusion coefficients ratio can be assumed with respect to α phase. This assumption reflects small layer thickness of this phase and vice versa. The optimum choice of diffusion coefficient ratios are $\Delta_\alpha = 3.2 \times 10^4$, $\Delta_{\beta_1} = 1 \times 10^3$, $\Delta_\gamma = 60$, $\Delta_\delta = 6$ and $\Delta_L = 1$ with $D_L = 5.3 \times 10^{-11}\ m^2/s$. Thus, $D_\alpha = 1.656 \times 10^{-15}\ m^2/s$, $D_{\beta_1} = 5.3 \times 10^{-14}\ m^2/s$, $D_\gamma = 8.833 \times 10^{-13}\ m^2/s$ and $D_\delta = 8.833 \times 10^{-12}\ m^2/s$. These values can be applied to the system of four nonlinear equations and then solved numerically for $\eta_{\alpha\beta_1}$,$\eta_{\beta_1\gamma}, \eta_{\gamma\delta}$ and $\eta_{\delta L}$. The solution gives the values of the rate constants as follow: $\eta_{\alpha\beta_1} = 0.2346 \times 10^{-03}$, $\eta_{\beta_1\gamma} = 0.1412 \times 10^{-02}, \eta_{\gamma\delta} = 0.4283 \times 10^{-01}$ and $\eta_{\delta L} = 0.9273 \times 10^{-01}$. These values designate the speed of the propagating interfaces; the higher the value the higher the propagation speed. The values of rate constants are sensitive to the value of diffusion coefficient ratios. Figure (12) represents the self-similar solution of the concentration profiles of phases $\alpha, \beta_1, \gamma, \delta$ and liquid Zn in the Ni-Zn diffusion couple. The ordinate indicates the concentration value of

Ni element while the abscissa represents the similarity variable η. Obviously, the concentration is discontinued at the rate constant values which are representing the location of the interfaces.

This representation can be transformed into time and distance scale. Figures 13, 14, 15, 16 and 18 show comparisons between model result and the experimental composition determined using the electron dispersive spectroscopy (EDS) for the Ni-Zn diffusion couple at 450^0C at 1 hour, 2 hours, 4 hours, 8 hours and 16 hours exposure times, respectively. Figures 17 and 19 are plotted to magnify phases $\alpha$and β_1 of the Ni-Zn system for 8 and 16 hours exposure time; although the experimental data points are few in the first and second phases, the model is matching very well with these points. The solid blue lines represent the calculated values while the red circles represent the experimental data points.

The model results show a very good representation of the compositional profile when compared with the experimental data despite the fact that in some phases, the concentration is not reaching equilibrium because of the quenching process. On the other hand, the interfaces' locations $\varphi_{\alpha\beta_1}, \varphi_{\beta_1\gamma}, \varphi_{\gamma\delta}$ and $\varphi_{\delta L}$ are plotted with different exposure time as illustrated in Figure (20). The interfaces' locations $\varphi_{\gamma\delta}$ and $\varphi_{\delta L}$ are compared with the experimental measurements as illustrated in Figure (20). In this Figure, the solid line represents the model results while the data points indicate the average of five fields' experimental measurements. An excellent agreement can be concluded from this Figure.

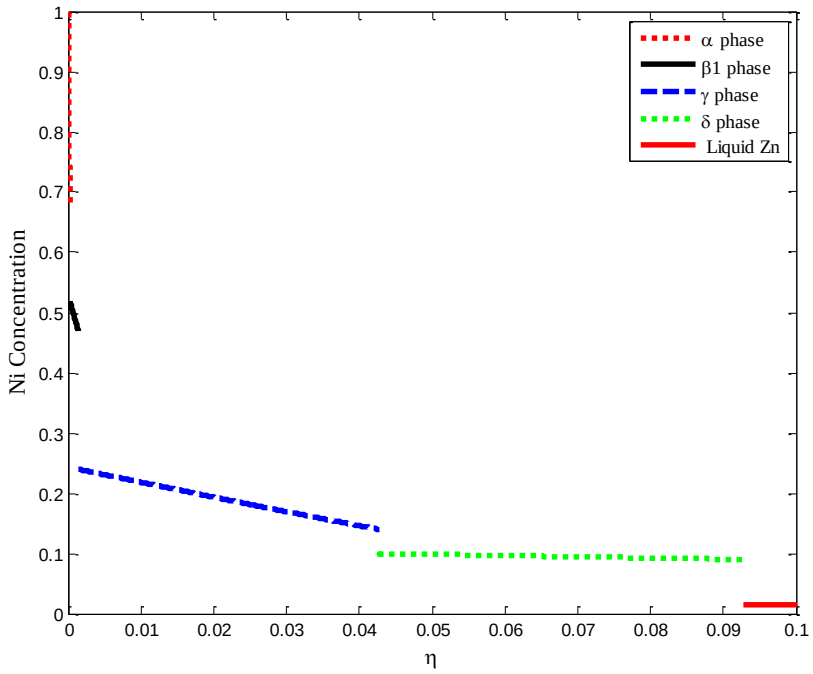

Figure 12. The model concentration profile of Ni-Zn diffusion couple based on similarity solution.

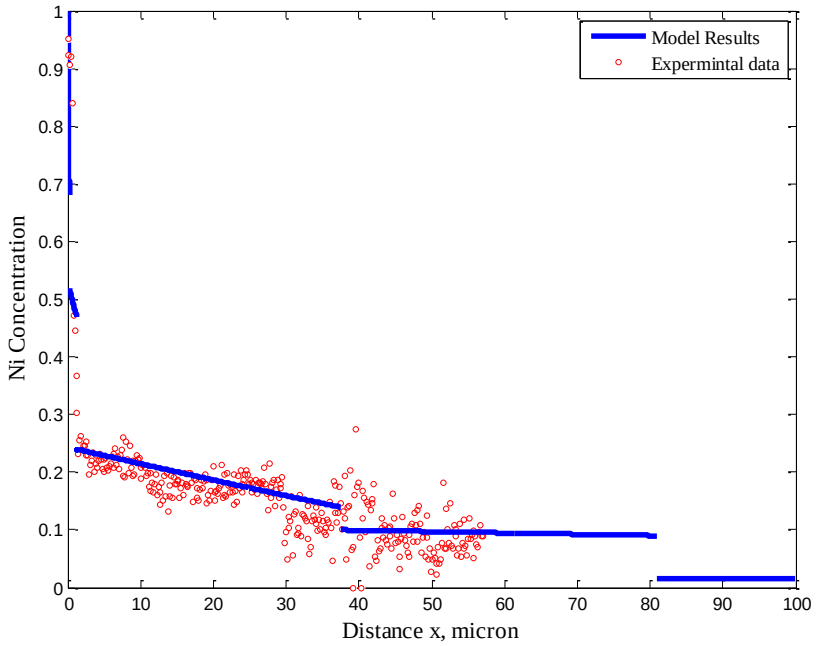

Figure 13. Measure and predicted concentration profile of Ni-Zn diffusion at 450^0C for 1 hours exposure time.

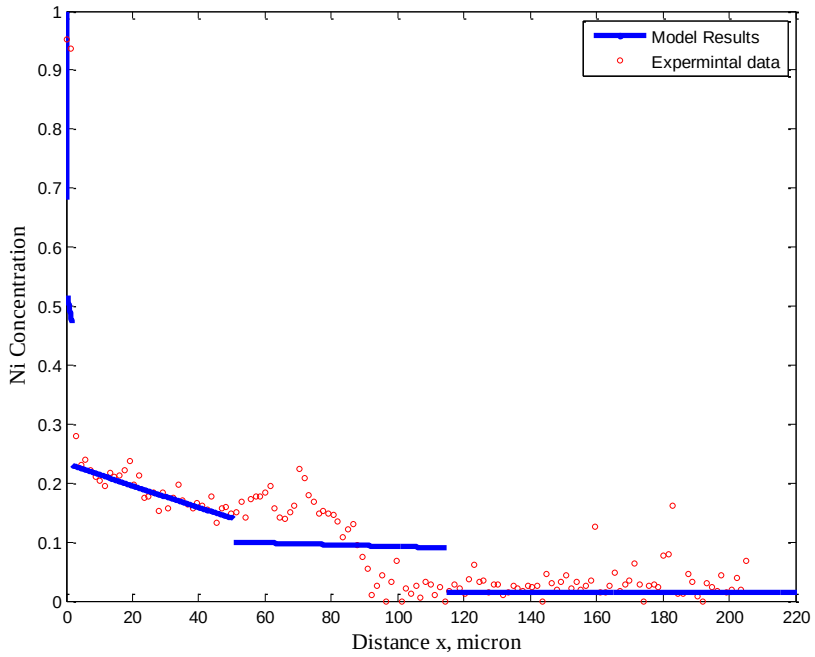

Figure 14. Measure and predicted concentration profile of Ni-Zn diffusion at 450^0C for 2 hours exposure time.

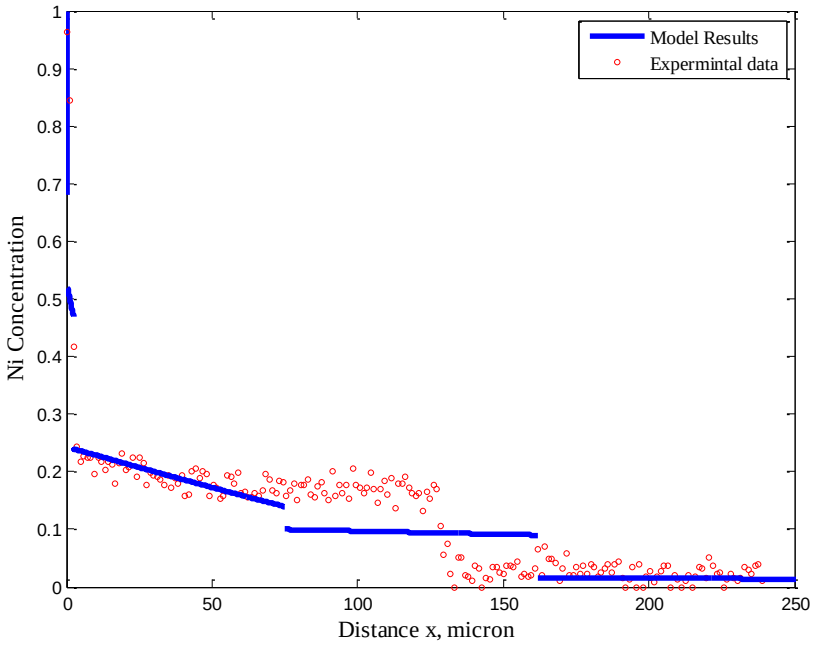

Figure 15. Measure and predicted concentration profile of Ni-Zn diffusion at 450^0C for 4 hours exposure time.

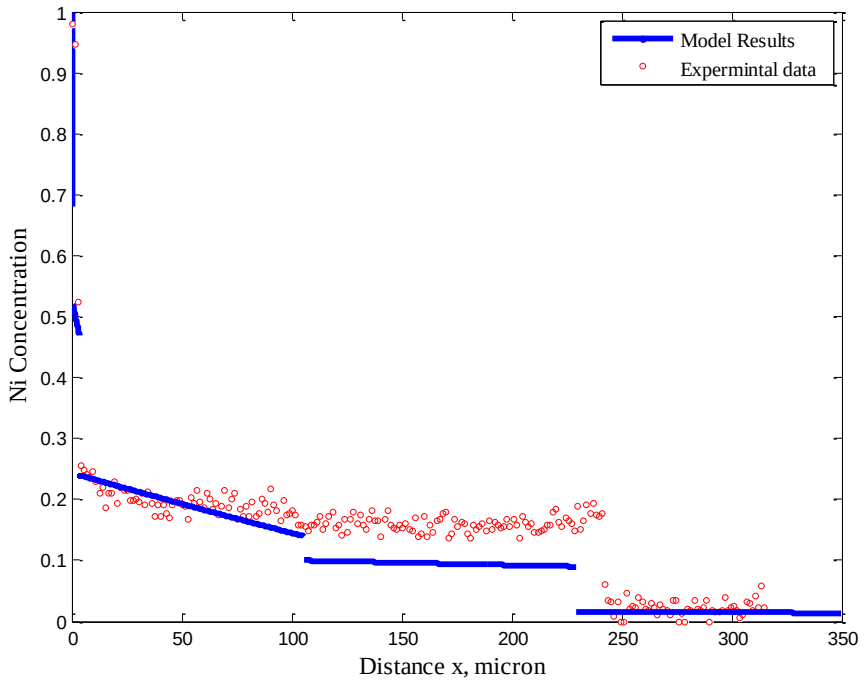

Figure 16. Measure and predicted concentration profile of Ni-Zn diffusion at 450^0C for 8 hours exposure time.

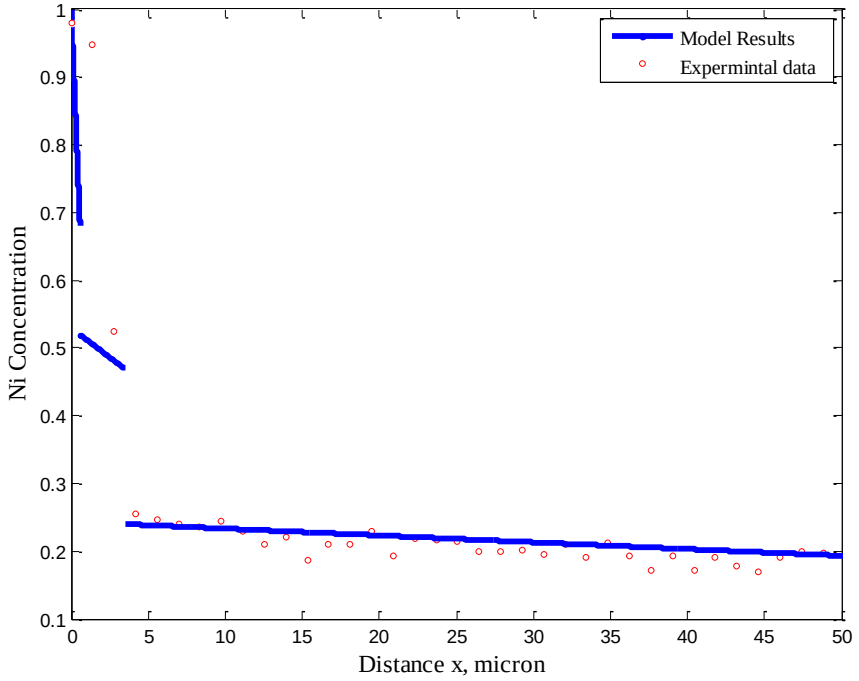

Figure 17. A magnification of the phases α and β_1 at 8 hours exposure time.

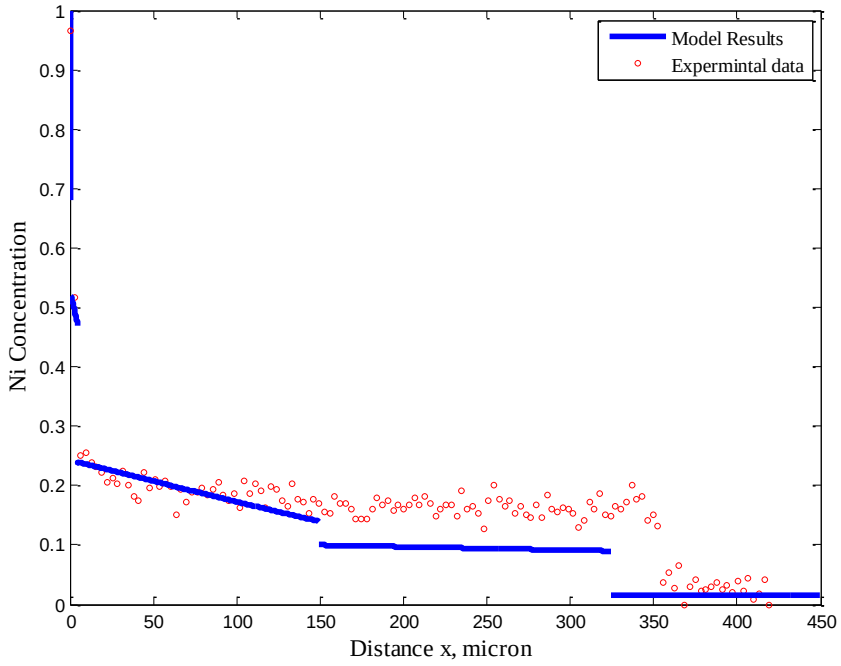

Figure 18. Measure and predicted concentration profile of Ni-Zn diffusion at 450^0C for 16 hours exposure time.

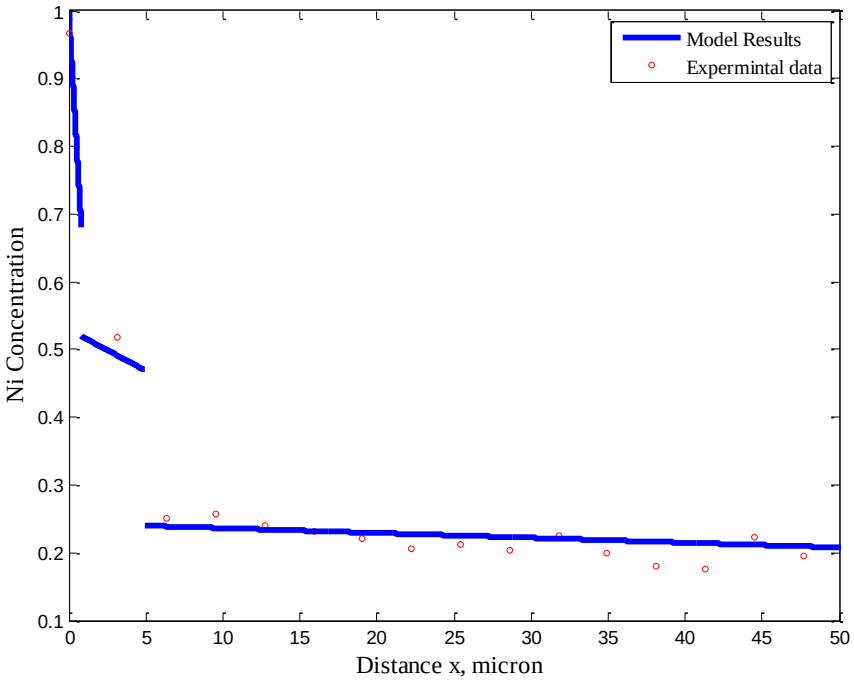

Figure 19. A magnification of the phases α and β_1 at 16 hours exposure time.

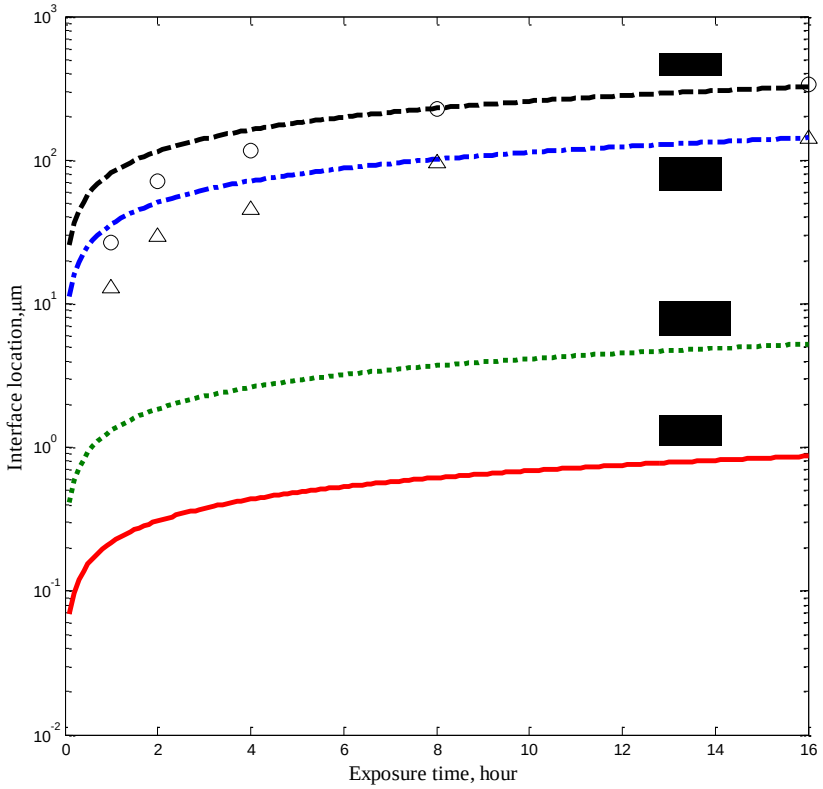

Figure 20. measured and predicted values of interfaces' locations of a Ni-Zn diffusion couple at 450C for different exposure times.

5.3 Multiple phase Model: Cu-Zn Binary System

Another case for a multiple phase model is the Cu-Zn binary system. According to the Cu-Zn binary phase diagram shown in Figure (21), this binary system has four phases: α, β', γ and ε appear to be stable phases at 450^0C. Likewise, a transition region between each two single phase region represents the propagation front.

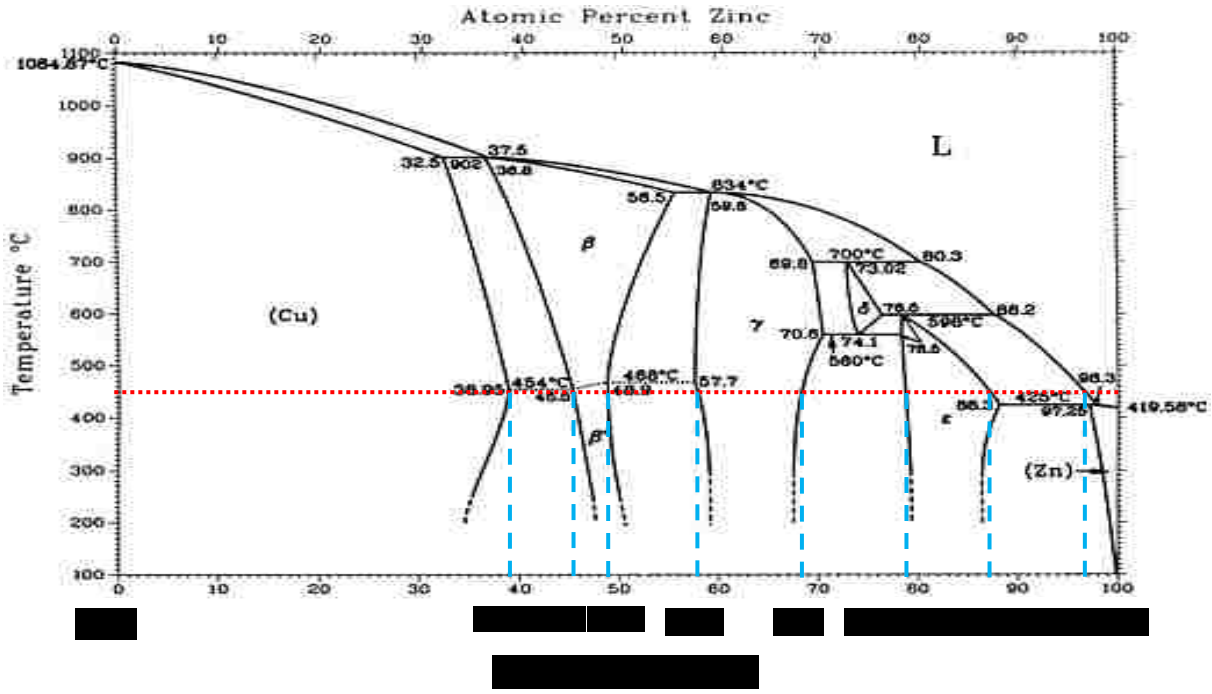

Figure 21. Cu-Zn equilibrium phase diagram [51].

Following an approach similar to that in Ni-Zn system, a system of four discontinuity equations describes the relationship between the constant concentration values and the rate constants. The resultant equations are coupled with four independent variables $\eta_{\alpha\beta'}$,$\eta_{\beta'\gamma}$, $\eta_{\gamma\varepsilon}$ and $\eta_{\varepsilon L}$. Referring to Figure (21), the dotted red line represents the temperature level line at 450^{0}C. Clearly, along this line, the concentration at the four interfaces and boundaries are illustrated in Figure (21). The values of ($c_{Cu\,\alpha}, c_{\alpha\beta'}, c_{\beta'\alpha}$, $c_{\beta'\gamma}, c_{\gamma\beta'}, c_{\gamma\varepsilon}$, $c_{\varepsilon\gamma}$, $c_{\varepsilon L}, c_{L\varepsilon}$ and $c_{L\,zn}$) are approximately (1.0, 0.61, 0.55, 0.515, 0.425, 0.315, 0.215, 0.125, 0.035 and 0).

The ratios of the diffusion coefficient, $\Delta_\alpha, \Delta_{\beta'}, \Delta_\gamma, \Delta_\varepsilon$ and Δ_L are selected to obtain best fit to the experimentally measured thickness of each phase. The values for the diffusion coefficient ratios are $\Delta_\alpha = 1.5 \times 10^4$, $\Delta_{\beta'} = 2.8 \times 10^3$, $\Delta_\gamma = 1.21 \times$

10^2 , $\Delta_\varepsilon = 3.35 \times 10^2$ and $\Delta_L = 1$ with $D_L = 6.7 \times 10^{-09}\, m^2/s$. Figure (22) represents the self-similar solution of the concentration profiles of phases $\alpha, \beta', \gamma, \varepsilon$ and liquid Zn in the Cu-Zn diffusion couple. The ordinate indicates the concentration value of Ni element while the abscissa represents the similarity variable η. Noticeably, the concentration is discontinued at the rate constant values which are representing the location of the interfaces. Note that the diffusion coefficient ratio Δ_ε is higher than Δ_γ which reflects the smaller thickness of the ε phase as can be seen in Figure (23).

Figure (23) shows a comparison between the calculated concentration profile of Cu and the experimental composition determined using the electron dispersive spectroscopy (EDS) at 8 hours exposure time. The solid lines represent the calculated values while the data points represent the experimental data. The model results show a very good representation of the compositional profile when compared with the available experimental data. The values of the diffusion coefficients in various phases are $D_\alpha = 4.467 \times 10^{-13}\, m^2/s$, $D_{\beta'} = 2.393 \times 10^{-12}\, m^2/s$, $D_\gamma = 5.537 \times 10^{-11}\, m^2/s$ and $D_\varepsilon = 2.0 \times 10^{-11}\, m^2/s$. Substituting these values to the system of four nonlinear discontinuity equations makes this system ready to solve numerically for $\eta_{\alpha\beta'}$,$\eta_{\beta'\gamma}$, $\eta_{\gamma\varepsilon}$ and $\eta_{\varepsilon L}$. The rate constants are calculated to be $\eta_{\alpha\beta'} = 0.4779 \times 10^{-03}$, $\eta_{\beta'\gamma} = 0.7085 \times 10^{-03}$, $\eta_{\gamma\varepsilon} = 0.1775 \times 10^{-01}$ and $\eta_{\varepsilon L} = 0.2350 \times 10^{-01}$. Likewise, these values are dependent strongly on the values of diffusion coefficient ratios..

The model results for the interfaces' locations are $\varphi_{\alpha\beta'} = 13.28\, \mu m$, $\varphi_{\beta'\gamma} = 19.68\, \mu m$, $\varphi_{\gamma\varepsilon} = 460\, \mu m$ and $\varphi_{\varepsilon L} = 652\, \mu m$. From the experimental measurements, the only observable phase interfaces are $\varphi_{\beta'\gamma}$, $\varphi_{\gamma\varepsilon}$ and $\varphi_{\varepsilon L}$ and their values are

17.16 μm, 489.1 μm and 652 μm, respectively. These values can be shown in Figure (24). The layer thickness corresponding to α phase is too small to be observed in the experiments due to the resolution of the optical microscope. The rate constants predicted for all three binary systems (Al-Zn, Ni-Zn, Cu-Zn) are verified by obtaining solutions using collocation method. The set of nonlinear ordinary differential equations (14, 15 and 35) are solved by the collocation method by treating the unknown locations of propagating fronts as eigenvalues of the system. Results obtained by such method agree perfectly with that presented in this paper using *Maple ™ 15* program.

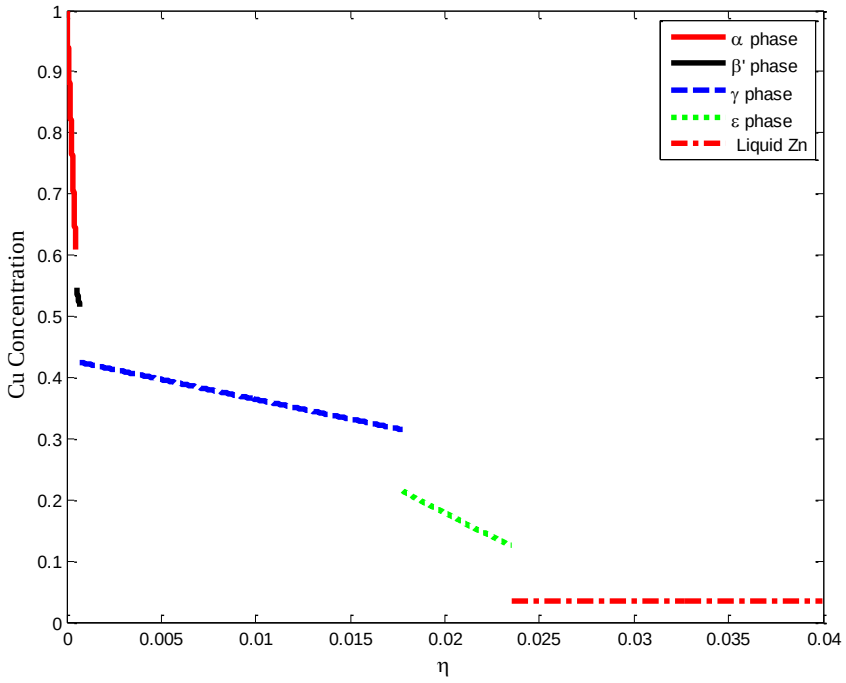

Figure 22. Concentration profile of the Cu-Zn diffusion couple based on self-similar solution.

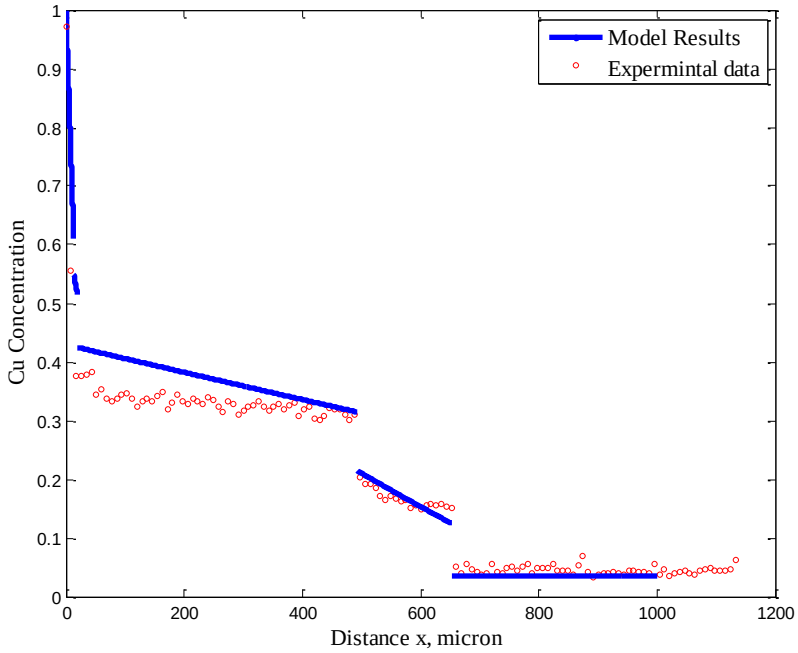

Figure 23. Measure and predicted concentration profile of Cu-Zn diffusion at 450^0C for 8 hour exposure time.

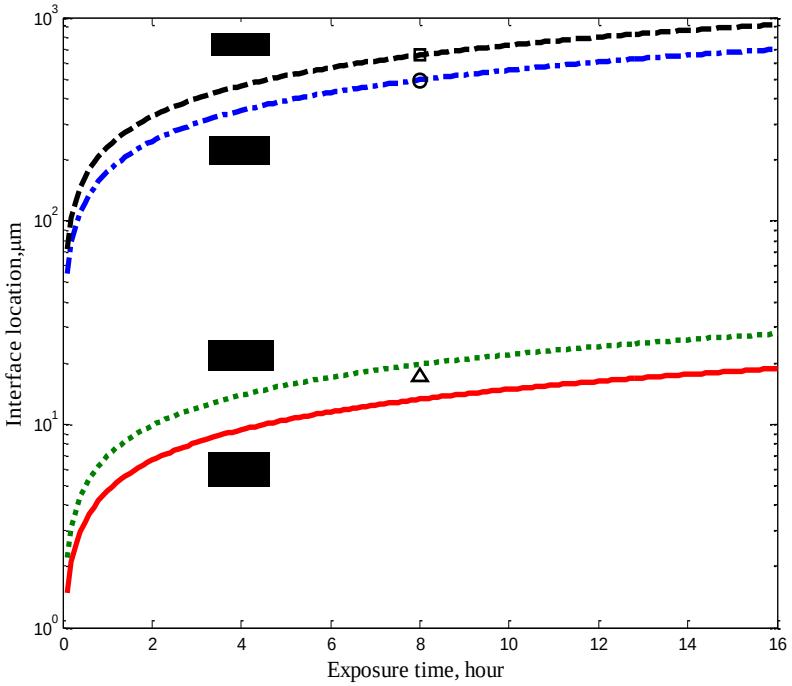

Figure 24. The experimental data for the interfaces' locations of Cu-Zn diffusion couple at 450^0C for 8 hour exposure time and model representation for different exposure time.

6 CHAPTER 6: CONCLUSIONS

In the present study, a diffusion model for various binary systems with multiple phases has been introduced based on a self-similar solution. A similarity variable is used to reduce the coupled set of nonlinear partial differential diffusion equations to a set of coupled nonlinear ordinary differential equations. The equations predicting the location of propagation fronts are reduced to the set of nonlinear algebraic equations and were solved using *Maple™ 15*.

The model was applied and compared with the experimental data for the Ni-Zn and Cu-Zn binary systems. System of equations of rate constants was solved for propagating fronts. The concentration values at the boundaries are directly related to the equilibrium phase diagram for such binary systems. In general, the model is capable of being applied to different binary systems. It is concluded that this model is presenting a very good agreement with the experimental data in terms of concentration profiles and interfaces' locations. Moreover, the phases' thicknesses can be easily determined by the proposed solution. More significantly, the model provides estimation for the diffusion coefficients in each phase. The diffusion coefficients are very low in the solid phases compared with the liquid phase.

Although two or three phases were observed in our investigation because other phases are extremely small in thicknesses, the model is able to detect these layers and estimate their thicknesses.

REFERENCES

[1] Anonymous (2011, Exploring thermal energy storage. *Altenergymag* Available: http://www.altenergymag.com/emagazine.php?art_id=1655.

[2] M. M. Farid, A. M. Khudhair, S. A. K. Razack and S. Al-Hallaj, "A review on phase change energy storage: Materials and applications," *Energy Conversion and Management,* vol. 45, pp. 1597-1615, 2004.

[3] Anonymous (2011, Encapsulated PCMs: How they work. *Microtechlabs* [online]. *2010(June/28),* Available: http://www.microteklabs.com/how-they-work.html.

[4] B. Lustman and R. F. Mehl, "Rate of Growth of Intermediate Alloy Layers in Structurally Analogous Systems," *Trans. Met. Soc. AIME,* vol. 147, pp. 369, 1942.

[5] D. Horstmann, "The attack of iron-saturated zinc melts upon iron," *Stahl. u. Eisen.,* vol. 73, pp. 659, 1953.

[6] S. Storchheim, J. L. Zambrow and H. H. Hausner, "Solid State Bonding of Aluminum to Nickel," *Trans. Met. Soc. AIME,* vol. 200, pp. 269, 1954.

[7] G. V. Kidson and G. D. Miller, "The interdiffusion of aluminum and zirconium," *J. Nucl. Mater.,* vol. 12, pp. 61, 1964.

[8] K. Shibata, S. Morozumi and S. Koda, "Formation of the alloy layer in the Fe-Al diffusion couple," *J. Jpn. Inst. Met.,* vol. 30, pp. 382, 1966.

[9] K. Hirano and Y. Ipposhi, "Interdiffusion in alloys III. Interdiffusion in iron-titanium systems," *J. Jpn. Inst. Met.,* vol. 32, pp. 815, 1968.

[10] M. M. P. Janssen, "Diffusion in the nickel-rich part of the Ni-Al system at 1000° to 1300°C; Ni_3Al layer growth, diffusion coefficients, and interface concentrations," *Metall. Mater. Trans. B,* vol. 4, pp. 1623, 1973.

[11] G. F. Bastin and G. D. Rieck, "Diffusion in the Titanium-Nickel Systems--1,2, Occurrence and Growth of the Various Intermetallic Compounds," *Metall. Mater. Trans. B,* vol. 5, pp. 1817-1831, 1974.

[12] M. Onishi and H. Fujibuchi, "Reaction-Diffusion in the Cu-Sn system," *Trans. Jpn. Inst. Met.,* vol. 16, pp. 539-547, 1975.

[13] E. Hannech and C. R. Hall, "Diffusion controlled reactions in gold/lead-tin solder system," *Mater. Sci. Technol.,* vol. 8, pp. 817, 1992.

[14] P. T. Vianco, P. F. Hlava and J. Kilgo, "Intermetallic compound layer formation between copper and hot-dipped 100In, 50In-50Sn, 100Sn, and 63Sn-37Pb coatings," *J. Electron. Mater.*, vol. 23, pp. 583, 1994.

[15] M. Watanabe, Z. Horita and M. Nemoto, "Analytical electron microscopy study of diffusion-bonded multiphase system," *Inteface Sci.*, vol. 4, pp. 229-241, 1996.

[16] S. Choi, T. R. Bieler, J. P. Lucas and K. N. Subramanian, "Characterization of the growth of intermetallic interfacial layers of Sn-Ag and Sn-Pb eutectic solders and their composite solders on Cu substrate during sothermal long-term aging," *J. Electron. Mater.*, vol. 28, pp. 1209, 1999.

[17] M. Kajihara, T. Yamada, K. Miura, N. Kurokawa and K. Sakamoto, "Morphology of compound layers at Au/Sn interface formed by reactive diffusion," *Netsushori.*, vol. 43, pp. 297, 2003.

[18] M. Kajihara, "Analysis of kinetics of reactive diffusion in a hypothetical binary system," *Acta Mater.*, vol. 52, pp. 1193-1200, 2004.

[19] T. Yamada, K. Miura, M. Kajihara, N. Kurokawa and K. Sakamoto, "Formation of intermetallic compound layers in Sn/Au/Sn diffusion couple during annealing at 433 K," *J. Mater. Sci.*, vol. 39, pp. 2327-2334, 2004.

[20] T. Yamada, K. Miura, M. Kajihara, N. Kurokawa and K. Sakamoto, "Kinetics of reactive diffusion between Au and Sn during annealing at solid-state temperatures," *Mater. Sci. Eng. , A*, vol. 390, pp. 118-126, 2005.

[21] M. Mita, M. Kajihara, N. Kurokawa and K. Sakamoto, "Growth behavior of Ni3Sn4 layer during reactive diffusion between Ni and Sn at solid-state temperatures," *Mater. Sci. Eng. , A*, vol. 403, pp. 269-275, 2005.

[22] Y. Muranishi and M. Kajihara, "Growth behavior of Nb3Sn layer during reactive diffusion between Cu-8.3Sn alloy and Nb," *Mater. Sci. Eng. , A*, vol. 404, pp. 33-41, 2005.

[23] K. Suzuki, S. Kano, M. Kajihara, N. Kurokawa and K. Sakamoto, "Reactive diffusion between Ag and Sn at solid state temperatures," *Mater. Trans.*, vol. 46, pp. 969, 2005.

[24] T. Takenaka, S. Kano, M. Kajihara, N. Kurokawa and K. Sakamoto, "Growth behavior of Au-Sn and Ag-Sn compounds during solid-state reactive diffusion between Au-Ag alloys and Sn," *Mater. Trans.*, vol. 46, pp. 1825, 2005.

[25] T. Takenaka, M. Kajihara, N. Kurokawa and K. Sakamoto, "Reactive diffusion between Pd and Sn at solid-state temperatures," *Mater. Sci. Eng. , A*, vol. 406, pp. 134-141, 2005.

[26] T. Takenaka, S. Kano, M. Kajihara, N. Kurokawa and K. Sakamoto, "Growth behavior of compound layers in Sn/Cu/Sn diffusion couples during annealing at 433-473 K," *Mater. Sci. Eng. , A,* vol. 396, pp. 115-123, 2005.

[27] T. Takenaka, M. Kajihara, N. Kurokawa and K. Sakamoto, "Reactive diffusion between Ag-Au alloys and Sn at solid-state temperatures," *Mater. Sci. Eng. , A,* vol. 427, pp. 210-222, 2006.

[28] T. Takenaka and M. Kajihara, "Evaluation of interdiffusion in liquid phase during reactive diffusion between Cu and Al," *Mater. Trans.,* vol. 47, pp. 822, 2006.

[29] T. Hayase and M. Kajihara, "Kinetics of reactive diffusion between Cu-8.1Sn-0.3Ti alloy and Nb," *Mater. Sci. Eng. , A,* vol. 433, pp. 83-89, 2006.

[30] M. Mita, K. Miura, T. Takenaka, M. Kajihara, N. Kurokawa and K. Sakamoto, "Effect of Ni on reactive diffusion between Au and Sn at solid-state temperatures," *Mater. Sci. Eng. , B,* vol. 126, pp. 37-43, 2006.

[31] Y. Yato and M. Kajihara, "Kinetics of reactive diffusion in the (Au-Ni)/Sn system at solid-state temperatures," *Mater. Sci. Eng. , A,* vol. 428, pp. 276-283, 2006.

[32] M. Kajihara and T. Takenaka, "Kinetic features of solid-state reactive diffusion between au and sn-base solder," in *5th International Conference on Processing and Manufacturing of Advanced Materials - THERMEC'2006, July 4, 2006 - July 8,* 2007, pp. 2473-2478.

[33] Y. Tanaka and M. Kajihara, "Numerical analysis for migration of interface between liquid and solid phases during reactive diffusion in the binary Cu-Al system," *Mater. Sci. Eng. , A,* vol. 459, pp. 101-110, 2007.

[34] Y. Tanaka, M. Kajihara and Y. Watanabe, "Growth behavior of compound layers during reactive diffusion between solid Cu and liquid Al," *Mater. Sci. Eng. , A,* vol. 445-446, pp. 355-363, 2007.

[35] Y. Yato and M. Kajihara, "Kinetic features of reactive diffusion between Sn-5Au alloy and Ni at solid-state temperatures," *Mater. Trans.,* vol. 47, pp. 2277, 2006.

[36] L. S. Castleman and L. L. Seigle, "Formation of Intermetallic Layers in Diffusion Couple," *Trans. Met. Soc. AIME,* vol. 209, pp. 1173, 1957.

[37] L. S. Castleman and L. L. Seigle, "Layer Growth During Interdiffusion in The Aluminum-Nickel Alloy system," *Trans. Met. Soc. AIME,* vol. 212, pp. 589, 1958.

[38] N. L. Peterson and R. E. Ogilvie, "Diffusion studies in the uranium-niobium system," *Trans. Met. Soc. AIME.,* vol. 218, pp. 439, 1960.

[39] Y. Adda, M. Beyeler, A. Kirianenko and M. F. Mauruce, "Determination of equilibrium diagrams by diffusion in the solid state," *Mem. Sci. Rev. Met.*, vol. 58, pp. 716, 1961.

[40] L. S. Birks and R. E. Seebold, "Diffusion of Nb with Cr, Fe, Ni, Mo, and stainless steel," *J. Nucl. Mater.*, vol. 3, pp. 249, 1961.

[41] R. E. Seebold and L. S. Birks, "Elevated temperature diffusion in the systems Nb-Pt, Nb-Se, Nb-Zn, Nb-Co, Ni-Ta, and Fe-Mo," *J. Nucl. Mater.*, vol. 3, pp. 260, 1961.

[42] J. W. E. Sweeney and A. P. Batt, "Electron probe and x-ray diffraction measurements of intermediate phases in Zr diffused with Cr, Fe, Ni, Cu, and Mo," *J. Nucl. Mater.*, vol. 13, pp. 87, 1964.

[43] T. Nishizawa and A. Chiba, "Phenomenological consideration on interphase equilibrium in diffusion couple," *J. Jpn. Inst. Met.*, vol. 34, pp. 629, 1970.

[44] O. V. Duchenko, "Diffusional formation of intermetallic layers in the Ni-Zn reaction couple," *Metal Physics and Advanced Technologies*, vol. 19, pp. 349-354, 2001.

[45] Y. Tanaka and M. Kajihara, "Kinetics of isothermal reactive diffusion between solid Fe and liquid Al," *J. Mater. Sci.*, vol. 45, pp. 5676-5684, 2010.

[46] P. L. Schdev, *Self-Similarity and Beyond; Exact Solutions of Nonlinear Problems.* New York: Chapman & Hall/CRC, 2000.

[47] W. Jost, *Diffusion in Solid, Liquid, Gases.* New York: Academic press Inc, 1960.

[48] D. A. Porter and K. E. Easterling, *Phase Transformations in Metals and Alloys.* London: Chapman & Hall, 1992.

[49] J. L. Murray. (1983, "Binary phase diagrams," in *ASM Handbooks Online*Anonymous [online]. Available: http://products.asminternational.org/hbk/index.jsp.

[50] P. Nash and Y. Y. Pan. (1991, "Binary phase diagrams," in *ASM Handbooks Online*Anonymous [online]. Available: http://products.asminternational.org/hbk/index.jsp.

[51] A. P. Miodownik. (2002, "Binary phase diagrams," in *ASM Handbooks Online*Anonymous [online]. Available: http://products.asminternational.org/hbk/index.jsp.

APPENDIX A

A.1 Maple Code for the Al-Zn Case

```
> restart;
> C1 := 1; C2 := 0.33; C3 := 0.155; C4 := 0;
```

$$C_1 := 1$$

$$C_2 := 0.33$$

$$C_3 := 0.155$$

$$C_4 := 0$$

```
> γl := 1e2;
```

$$\gamma l := 100.$$

```
> C2 - C3 = (C4 - C3) exp(-η1^2) / (η1 sqrt(π) (1 - erf(η1))) - (C2 - C1) exp(-γl η1^2) / (η1 sqrt(γl π) erf(sqrt(γl) η1))
```

$$0.175 = -\frac{0.155\, e^{-\eta_1^2}}{\eta_1 \sqrt{\pi}\,\left(1 - \operatorname{erf}(\eta_1)\right)} + \frac{0.06700000000\, e^{-100.\,\eta_1^2}}{\eta_1 \sqrt{\pi}\,\operatorname{erf}(10.\,\eta_1)}$$

```
> fsolve( (3), η[1] = 0.01)
```

$$0.03240495775$$

```
> η1 := fsolve( (3), η[1] = 0.01)
```

$$\eta_1 := 0.03240495775$$

```
> cp1 := (C2 - C1) / erf(sqrt(γl) η1) · erf(sqrt(γl) η)
```

$$cp1 := -1.896698775\, \operatorname{erf}(10.\,\eta)$$

```
> C1 = C1 + cp1
```

$$C1 = 1 - 1.896698775\, \operatorname{erf}(10.\,\eta)$$

```
> CC1 := solve( (7), C1 );
```

$$CC1 := 1. - 1.896698775\, \operatorname{erf}(10.\,\eta)$$

```
> plot([CC1], η = 0..η1)
```

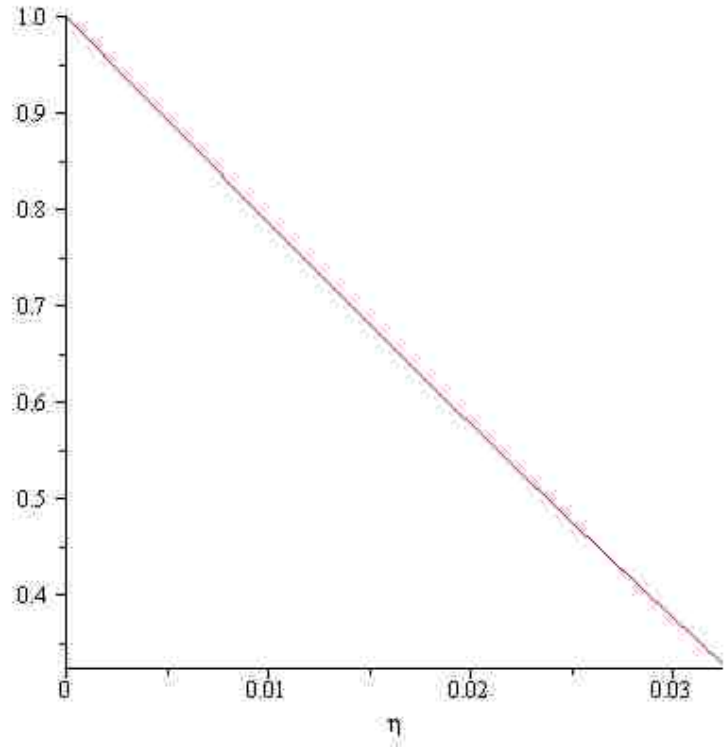

> $DD2 := \dfrac{2\cdot(C_4 - C_3)}{\sqrt{\pi}\cdot(1-\operatorname{erf}(\eta_1))}$

$$DD2 := -\frac{0.3217611034}{\sqrt{\pi}}$$

> $c1 = -DD2\cdot\int_{\eta}^{\infty} e^{-\eta^2}\,d\eta$

$$c1 = \frac{0.3217611034\left(-\frac{1}{2}\sqrt{\pi}\,\operatorname{erf}(\eta)+\frac{1}{2}\sqrt{\pi}\right)}{\sqrt{\pi}}$$

> $cc1 := solve(\ \mathbf{(10)}, c1\ )$

$$cc1 := -0.1608805517\,\operatorname{erf}(\eta) + 0.1608805517$$

> $plot([cc1], \eta = \eta_1 ..1)$

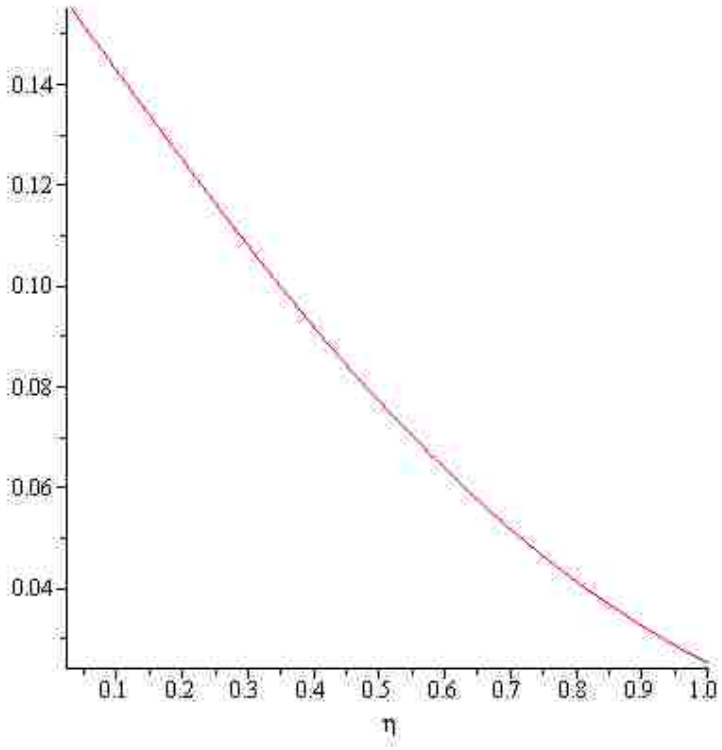

A.2 Maple Code for the Ni-Zn Case

> *restart*;

> $C_1 := 1; C_2 := 0.68; C_3 := 0.52; C_4 := 0.47; C_5 := 0.24; C_6 := 0.14; C_7 := 0.1; C_8 := 0.09; C_9 := 0.015; C_{10} := 0;$

$$C_1 := 1$$

$$C_2 := 0.68$$

$$C_3 := 0.52$$

$$C_4 := 0.47$$

$$C_5 := 0.24$$

$$C_6 := 0.14$$

$$C_7 := 0.1$$

$$C_8 := 0.09$$

$$C_9 := 0.015$$

$$C_{10} := 0$$

> $De := 0.53 \cdot 1e2;$

$$De := 53.$$

> $\gamma 1 := 32000;$

$$\gamma 1 := 32000$$

> $\gamma 2 := 1000;$

$$\gamma 2 := 1000$$

> $\gamma 3 := 60;\ \gamma 4 := 6;$

$$\gamma 3 := 60$$

$$\gamma 4 := 6$$

> $Da := \frac{De}{\gamma 1};\ Db := \frac{De}{\gamma 2};\ Dc := \frac{De}{\gamma 3};\ Dd := \frac{De}{\gamma 4}$

$$Da := 0.001656250000$$

$$Db := 0.05300000000$$

$$Dc := 0.8833333333$$

$$Dd := 8.833333333$$

>

>

>

>

>

>

> $$eqn1 := C_2 - C_3 = \frac{\left(C_4 - C_3\right) e^{-\gamma 2\, \eta_1^2}}{\eta_1 \sqrt{\pi\, \gamma 2}\, \left(-\operatorname{erf}\left(\sqrt{\gamma 2}\, \eta_1\right) + \operatorname{erf}\left(\sqrt{\gamma 2}\, \eta_2\right)\right)} - \frac{\left(C_2 - C_1\right) e^{-\gamma 1\, \eta_1^2}}{\eta_1 \sqrt{\pi\, \gamma 1}\, \operatorname{erf}\left(\sqrt{\gamma 1}\, \eta_1\right)}$$

$$eqn1 := 0.16 = -\frac{0.0005000000000\, e^{-1000\, \eta_1^2} \sqrt{10}}{\eta_1 \sqrt{\pi}\, \left(-\operatorname{erf}\left(10 \sqrt{10}\, \eta_1\right) + \operatorname{erf}\left(10 \sqrt{10}\, \eta_2\right)\right)} + \frac{0.0008000000000\, e^{-32000\, \eta_1^2} \sqrt{5}}{\eta_1 \sqrt{\pi}\, \operatorname{erf}\left(80 \sqrt{5}\, \eta_1\right)}$$

> *simplify*(**(7)**)

$$0.1600000000 = \left(1.261566261\,10^{-12}\, e^{-1000.\,\eta_1^2} \left(7.07106781\,10^{8}\, \mathrm{erf}\left(178.885438 + 8.00000000\,10^{8}\, e^{-31000.\,\eta_1^2}\, \mathrm{erf}\left(31.62277659\,\eta_1 \right) - 8.00000000\,10^{8}\, e^{-31000.\,\eta_1^2}\, \mathrm{erf}\left(31.62277659\,\eta_2 \right) \right) \right) \right) \Big/ \left(\mathrm{erf}\left(178.8854382\,\eta_1 \right) \left(\mathrm{erf}\left(31.62277659\,\eta_1 \right) - 1.\,\mathrm{erf}\left(31.62277659\,\eta_2 \right) \right) \eta_1 \right)$$

>

>

> $$eqn2 := C_4 - C_5 = \frac{\left(C_6 - C_5 \right) e^{-\gamma 3\,\eta_2^2}}{\eta_2 \sqrt{\pi\,\gamma 3}\, \left(-\mathrm{erf}\left(\sqrt{\gamma 3}\,\eta_2 \right) + \mathrm{erf}\left(\sqrt{\gamma 3}\,\eta_3 \right) \right)} - \frac{\left(C_4 - C_3 \right) e^{-\gamma 2\,\eta_2^2}}{\eta_2 \sqrt{\pi\,\gamma 2}\, \left(-\mathrm{erf}\left(\sqrt{\gamma 2}\,\eta_1 \right) + \mathrm{erf}\left(\sqrt{\gamma 2}\,\eta_2 \right) \right)}$$

$$eqn2 := 0.23 = -\frac{0.003333333333\, e^{-60\,\eta_2^2 \sqrt{15}}}{\eta_2 \sqrt{\pi}\, \left(-\mathrm{erf}\left(2\sqrt{15}\,\eta_2 \right) + \mathrm{erf}\left(2\sqrt{15}\,\eta_3 \right) \right)} + \frac{0.0005000000000\, e^{-1000\,\eta_2^2 \sqrt{10}}}{\eta_2 \sqrt{\pi}\, \left(-\mathrm{erf}\left(10\sqrt{10}\,\eta_1 \right) + \mathrm{erf}\left(10\sqrt{10}\,\eta_2 \right) \right)}$$

> *simplify*(**(9)**)

$$0.2300000000 = \left(2.000000000\,10^{-13} \left(3.641828102\,10^{10}\, e^{-60.\,\eta_2^2}\, \mathrm{erf}\left(31.6227765 - 3.641828102\,10^{10}\, e^{-60.\,\eta_2^2}\, \mathrm{erf}\left(31.62277659\,\eta_2 \right) - 4.460310289\,10^{9}\, e^{-1000.\,\eta_2^2}\, \mathrm{erf}\left(7.745966692\,\eta_2 \right) + 4.460310289\,10^{9}\, e^{-1000.\,\eta_2^2}\, \mathrm{erf}\left(7.745966692\,\eta_3 \right) \right) \right) \Big/ \left(\left(\mathrm{erf}\left(31.62277659\,\eta_1 \right) - 1.\,\mathrm{erf}\left(31.62277659\,\eta_2 \right) \right) \left(\mathrm{erf}\left(7.745966692\,\eta_2 \right) - 1.\,\mathrm{erf}\left(7.745966692\,\eta_3 \right) \right) \eta_2 \right)$$

> $$eqn3 := C_6 - C_7 = \frac{\left(C_8 - C_7\right) e^{-\gamma 4 \cdot \eta_3^2}}{\eta_3 \sqrt{\pi\, \gamma 4}\, \left(-\operatorname{erf}\left(\sqrt{\gamma 4}\, \eta_3\right) + \operatorname{erf}\left(\sqrt{\gamma 4}\, \eta_4\right)\right)} - \frac{\left(C_6 - C_5\right) e^{-\gamma 3\, \eta_3^2}}{\eta_3 \sqrt{\pi\, \gamma 3}\, \left(-\operatorname{erf}\left(\sqrt{\gamma 3}\, \eta_2\right) + \operatorname{erf}\left(\sqrt{\gamma 3}\, \eta_3\right)\right)}$$

$$eqn3 := 0.04 = -\frac{0.001666666667\, e^{-6\, \eta_3^2} \sqrt{6}}{\eta_3 \sqrt{\pi}\, \left(-\operatorname{erf}\left(\sqrt{6}\, \eta_3\right) + \operatorname{erf}\left(\sqrt{6}\, \eta_4\right)\right)} + \frac{0.003333333333\, e^{-60\, \eta_3^2} \sqrt{15}}{\eta_3 \sqrt{\pi}\, \left(-\operatorname{erf}\left(2 \sqrt{15}\, \eta_2\right) + \operatorname{erf}\left(2 \sqrt{15}\, \eta_3\right)\right)}$$

> *simplify*(**(13)**)

$$0.07500000000 = -\left(1.128379167\, 10^{-12} e^{-1.\, \eta_4^2} \left(-7.500000000\, 10^9 \operatorname{erf}\left(2.449489743\, \eta_3\right) + 7.500000000\, 10^9 \operatorname{erf}\left(2.449489743\, \eta_4\right) - 2.041241453\, 10^9 e^{-5.\, \eta_4^2} + 2.041241453\, 10^9 e^{-5.\, \eta_4^2} \operatorname{erf}\left(\eta_4\right)\right)\right) \Big/ \left(\left(\operatorname{erf}\left(2.449489743\, \eta_3\right) - 1.\, \operatorname{erf}\left(2.449489743\, \eta_4\right)\right) \left(-1. + \operatorname{erf}\left(\eta_4\right)\right) \eta_4\right)$$

> $$eqn4 := C_8 - C_9 = \frac{\left(C_{10} - C_9\right) e^{-\eta_4^2}}{\eta_4 \sqrt{\pi}\, \left(1 - \operatorname{erf}\left(\eta_4\right)\right)} - \frac{\left(C_8 - C_7\right) e^{-\gamma 4 \cdot \eta_4^2}}{\eta_4 \sqrt{\pi\, \gamma 4}\, \left(-\operatorname{erf}\left(\sqrt{\gamma 4}\, \eta_3\right) + \operatorname{erf}\left(\sqrt{\gamma 4}\, \eta_4\right)\right)}$$

$$eqn4 := 0.075 = -\frac{0.015\, e^{-\eta_4^2}}{\eta_4 \sqrt{\pi}\, \left(1 - \operatorname{erf}\left(\eta_4\right)\right)} + \frac{0.001666666667\, e^{-6\, \eta_4^2} \sqrt{6}}{\eta_4 \sqrt{\pi}\, \left(-\operatorname{erf}\left(\sqrt{6}\, \eta_3\right) + \operatorname{erf}\left(\sqrt{6}\, \eta_4\right)\right)}$$

> *simplify*(**(13)**)

$$0.07500000000 = -\left(1.128379167\,10^{-12}\,e^{-1.\,\eta_4^2}\left(-7.500000000\,10^{9}\,\mathrm{erf}\left(2.449489743\,\eta_3\right) + 7.500000000\,10^{9}\,\mathrm{erf}\left(2.449489743\,\eta_4\right) - 2.041241453\,10^{9}\,e^{-5.\,\eta_4^2} + 2.041241453\,10^{9}\,e^{-5.\,\eta_4^2}\,\mathrm{erf}\left(\eta_4\right)\right)\right) \Big/ \left(\left(\mathrm{erf}\left(2.449489743\,\eta_3\right) - 1.\,\mathrm{erf}\left(2.449489743\,\eta_4\right)\right)\left(-1. + \mathrm{erf}\left(\eta_4\right)\right)\eta_4\right)$$

> $\{eqn1, eqn2, eqn3, eqn4\}$

$$\left\{0.04 = -\frac{0.001666666667\,e^{-6\,\eta_3^2}\sqrt{6}}{\eta_3\sqrt{\pi}\left(-\mathrm{erf}\left(\sqrt{6}\,\eta_3\right) + \mathrm{erf}\left(\sqrt{6}\,\eta_4\right)\right)} + \frac{0.003333333333\,e^{-60\,\eta_3^2}\sqrt{15}}{\eta_3\sqrt{\pi}\left(-\mathrm{erf}\left(2\sqrt{15}\,\eta_2\right) + \mathrm{erf}\left(2\sqrt{15}\,\eta_3\right)\right)}, 0.075 = -\frac{0.015\,e^{-\eta_4^2}}{\eta_4\sqrt{\pi}\left(1 - \mathrm{erf}\left(\eta_4\right)\right)} + \frac{0.001666666667\,e^{-6\,\eta_4^2}\sqrt{6}}{\eta_4\sqrt{\pi}\left(-\mathrm{erf}\left(\sqrt{6}\,\eta_3\right) + \mathrm{erf}\left(\sqrt{6}\,\eta_4\right)\right)}, 0.16 = -\frac{0.0005000000000\,e^{-1000\,\eta_1^2}\sqrt{10}}{\eta_1\sqrt{\pi}\left(-\mathrm{erf}\left(10\sqrt{10}\,\eta_1\right) + \mathrm{erf}\left(10\sqrt{10}\,\eta_2\right)\right)} + \frac{0.0008000000000\,e^{-32000\,\eta_1^2}\sqrt{5}}{\eta_1\sqrt{\pi}\,\mathrm{erf}\left(80\sqrt{5}\,\eta_1\right)}, 0.23 = -\frac{0.003333333333\,e^{-60\,\eta_2^2}\sqrt{15}}{\eta_2\sqrt{\pi}\left(-\mathrm{erf}\left(2\sqrt{15}\,\eta_2\right) + \mathrm{erf}\left(2\sqrt{15}\,\eta_3\right)\right)} + \frac{0.0005000000000\,e^{-1000\,\eta_2^2}\sqrt{10}}{\eta_2\sqrt{\pi}\left(-\mathrm{erf}\left(10\sqrt{10}\,\eta_1\right) + \mathrm{erf}\left(10\sqrt{10}\,\eta_2\right)\right)}\right\}$$

> *fsolve*(**(15)**, $\{\eta[1] = 0.0002421197983, \eta[2] = 0.001457470263, \eta[3] = 0.03981975378, \eta[4] = 0.09036670427\}$)

$$\{\eta_1 = 0.0002345851149, \eta_2 = 0.001411831095, \eta_3 = 0.04282699008, \eta_4 = 0.09272817265\}$$

> $\eta_1 := 0.0002345851149; \eta_2 := 0.001411831095; \eta_3 := 0.04282699008; \eta_4 := 0.09272817265;$

$$\eta_1 := 0.0002345851149$$

$$\eta_2 := 0.001411831095$$

$$\eta_3 := 0.04282699008$$

$$\eta_4 := 0.09272817265$$

> $x44 := \eta_4 \cdot \sqrt{4 \cdot De \cdot 3600 \cdot 16}$

$$x44 := 324.0342176$$

> $x33 := \eta_3 \cdot \sqrt{4 \cdot De \cdot 3600 \cdot 16}$

$$x33 := 149.6568931$$

> $x22 := \eta_2 \cdot \sqrt{4 \cdot De \cdot 3600 \cdot 16}$

$$x22 := 4.933577048$$

> $x11 := \eta_1 \cdot \sqrt{4 \cdot De \cdot 3600 \cdot 16}$

$$x11 := 0.8197465992$$

>

> $DD1 := \frac{(C_2 - C_1)}{\operatorname{erf}\left(\sqrt{\gamma 1}\ \eta_1\right)} \cdot \operatorname{erf}\left(\sqrt{\gamma 1}\ \eta\right)$

$$DD1 := -\frac{0.32 \operatorname{erf}\left(80\sqrt{5}\ \eta\right)}{\operatorname{erf}\left(0.01876680919\sqrt{5}\right)}$$

> $c1 = C_1 + DD1$

$$c1 = 1 - \frac{0.32 \operatorname{erf}\left(80\sqrt{5}\ \eta\right)}{\operatorname{erf}\left(0.01876680919\sqrt{5}\right)}$$

> $solve(\ \mathbf{(23)}, c1\ )$

$$1.000000000 - 6.761987203 \operatorname{erf}(178.8854382\,\eta)$$

> $cc1 := solve(\ \mathbf{(23)}, c1\ )$

$$cc1 := 1.000000000 - 6.761987203 \operatorname{erf}(178.8854382\,\eta)$$

> $plot\left([cc1], \eta = 0..\eta_1\right)$

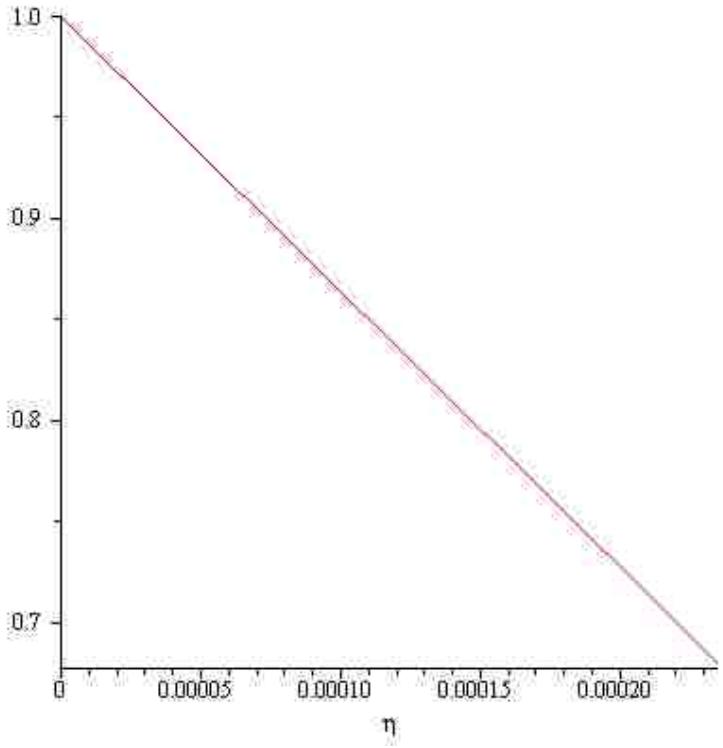

> $DD2 := \frac{(C_4 - C_3)}{-\mathrm{erf}\left(\sqrt{\gamma 2}\,\eta_1\right) + \mathrm{erf}\left(\sqrt{\gamma 2}\,\eta_2\right)} \cdot \left(\mathrm{erf}\left(\sqrt{\gamma 2}\,\eta\right) - \mathrm{erf}\left(\sqrt{\gamma 2}\,\eta_1\right)\right)$

$$DD2 := -\frac{0.05\left(\mathrm{erf}\left(10\sqrt{10}\,\eta\right) - \mathrm{erf}\left(0.002345851149\sqrt{10}\right)\right)}{-\mathrm{erf}\left(0.002345851149\sqrt{10}\right) + \mathrm{erf}\left(0.01411831095\sqrt{10}\right)}$$

> $c2 = C_3 + \mathrm{DD2}$

$$c2 = 0.52 - \frac{0.05\left(\mathrm{erf}\left(10\sqrt{10}\,\eta\right) - \mathrm{erf}\left(0.002345851149\sqrt{10}\right)\right)}{-\mathrm{erf}\left(0.002345851149\sqrt{10}\right) + \mathrm{erf}\left(0.01411831095\sqrt{10}\right)}$$

> $cc2 := solve(\ \mathbf{(27)}, c2\ );$

$$cc2 := 0.5299710219 - 1.191220408\,\mathrm{erf}\left(31.62277660\,\eta\right)$$

> $plot\left([cc2], \eta = \eta_1 .. \eta_2\right)$

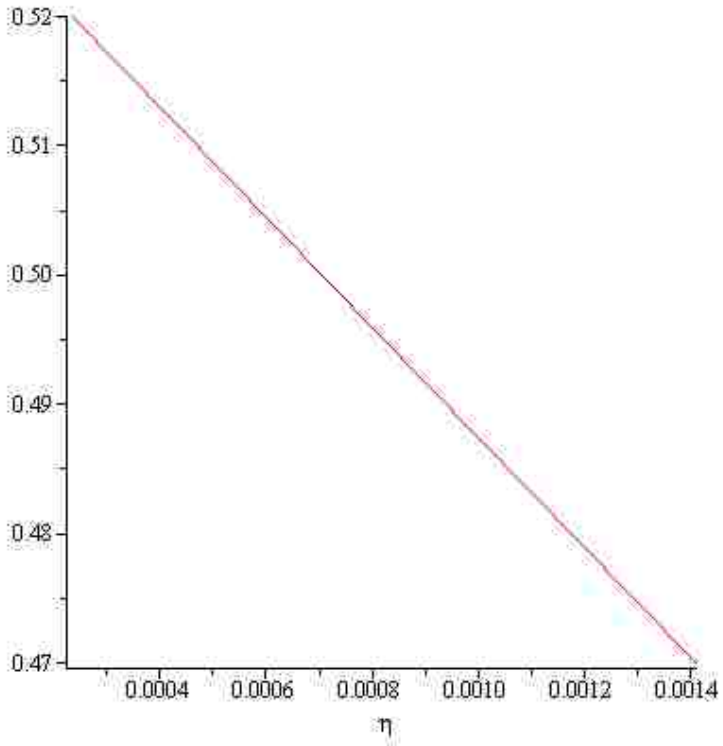

> $DD3 := \dfrac{(C_6 - C_5)}{-\mathrm{erf}\left(\sqrt{\gamma 3}\ \eta_2\right) + \mathrm{erf}\left(\sqrt{\gamma 3}\ \eta_3\right)} \cdot \left(\mathrm{erf}\left(\sqrt{\gamma 3}\ \eta\right) - \mathrm{erf}\left(\sqrt{\gamma 3}\ \eta_2\right)\right)$

$$DD3 := -\frac{0.10\left(\mathrm{erf}\left(2\sqrt{15}\ \eta\right) - \mathrm{erf}\left(0.002823662190\sqrt{15}\right)\right)}{-\mathrm{erf}\left(0.002823662190\sqrt{15}\right) + \mathrm{erf}\left(0.08565398016\sqrt{15}\right)}$$

> $c3 = C_5 + \mathrm{DD3}$

$$c3 = 0.24 - \frac{0.10\left(\mathrm{erf}\left(2\sqrt{15}\ \eta\right) - \mathrm{erf}\left(0.002823662190\sqrt{15}\right)\right)}{-\mathrm{erf}\left(0.002823662190\sqrt{15}\right) + \mathrm{erf}\left(0.08565398016\sqrt{15}\right)}$$

> $cc3 := solve(\ \mathbf{(30)}, c3);$

$$cc3 := 0.2435387503 - 0.2867832643\,\mathrm{erf}\left(7.745966692\,\eta\right)$$

> $plot\left([cc3], \eta = \eta_2 .. \eta_3\right)$

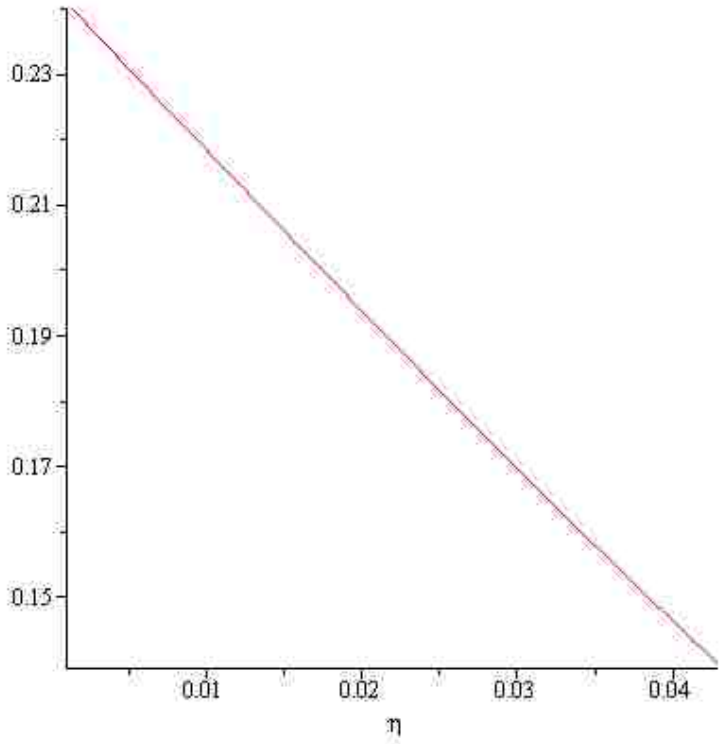

> $DD4 := \dfrac{(C_8 - C_7)}{-\mathrm{erf}\left(\sqrt{\gamma 4}\,\eta_3\right) + \mathrm{erf}\left(\sqrt{\gamma 4}\,\eta_4\right)} \cdot \left(\mathrm{erf}\left(\sqrt{\gamma 4}\,\eta\right) - \mathrm{erf}\left(\sqrt{\gamma 4}\,\eta_3\right)\right)$

$$DD4 := -\frac{0.01\left(\mathrm{erf}\left(\sqrt{6}\,\eta\right) - \mathrm{erf}\left(0.04282699008\sqrt{6}\right)\right)}{-\mathrm{erf}\left(0.04282699008\sqrt{6}\right) + \mathrm{erf}\left(0.09272817265\sqrt{6}\right)}$$

> $c4 = C_7 + DD4$

$$c4 = 0.1 - \frac{0.01\left(\mathrm{erf}\left(\sqrt{6}\,\eta\right) - \mathrm{erf}\left(0.04282699008\sqrt{6}\right)\right)}{-\mathrm{erf}\left(0.04282699008\sqrt{6}\right) + \mathrm{erf}\left(0.09272817265\sqrt{6}\right)}$$

> $cc4 := solve(\ (33), c4\ )$

$$cc4 := 0.1088002899 - 0.07461729972\,\mathrm{erf}\left(2.449489743\,\eta\right)$$

> $plot\left([cc4], \eta = \eta_3 .. \eta_4\right)$

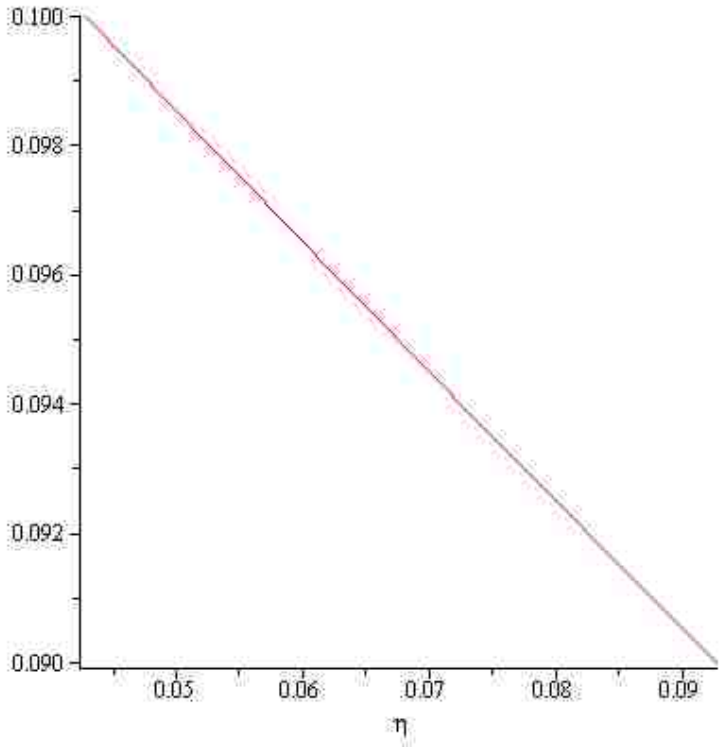

>

> $DD5 := \dfrac{2\cdot\left(C_{10}-C_9\right)}{\sqrt{\pi}\cdot\left(1-\operatorname{erf}\left(\eta_4\right)\right)}$

$$DD5 := -\frac{0.03349460672}{\sqrt{\pi}}$$

> $c5 = -DD5\cdot\int_{\eta}^{\infty} e^{-\eta^2}\,d\eta$

$$c5 = \frac{0.03349460672\left(-\frac{1}{2}\sqrt{\pi}\,\operatorname{erf}(\eta)+\frac{1}{2}\sqrt{\pi}\right)}{\sqrt{\pi}}$$

> $cc5 := solve(\ \mathbf{(36)}, c5)$

$$cc5 := -0.01674730336\,\operatorname{erf}(\eta)+0.01674730336$$

> $plot\left([cc5], \eta = \eta_4..6\right)$

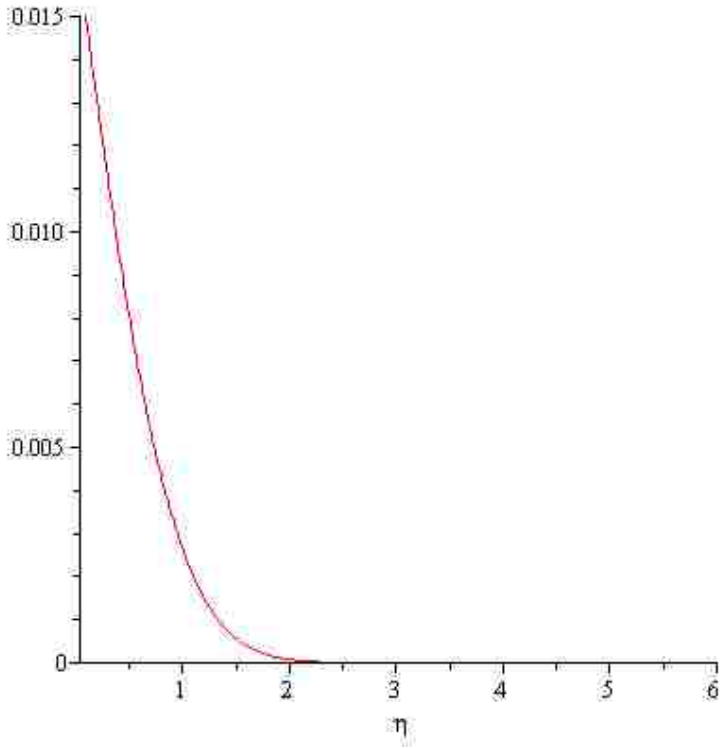

> $\eta := \frac{x}{\sqrt{4 \cdot De \cdot 3600 \cdot 16}};$

$$\eta := 0.0002861678415\,x$$

> *cc1*

$$1.000000000 - 6.761987203\,\mathrm{erf}(0.05119125973\,x)$$

> *plot*(**(39)**, $x = 0 .. x11$)

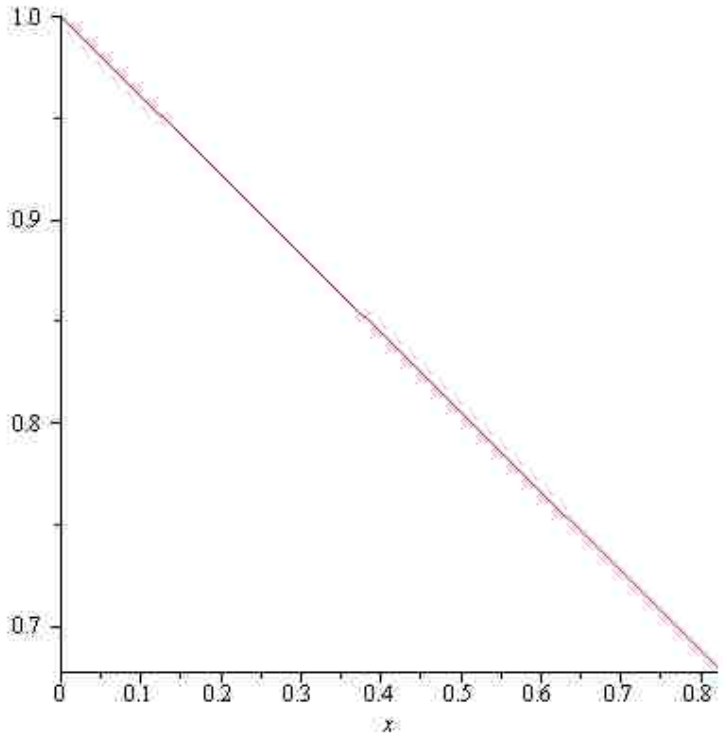

> *cc2*

$$0.5299710219 - 1.191220408\,\mathrm{erf}(0.009049421722\,x)$$

> *plot*(**(40)**, *x* = *x11* .. *x22*)

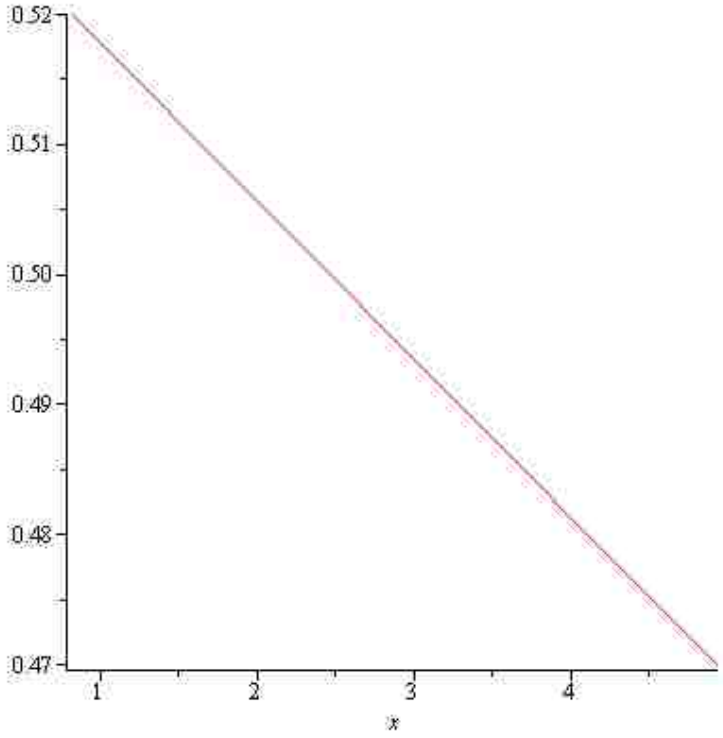

> *cc3*

$$0.2435387503 - 0.2867832643\,\mathrm{erf}(0.002216646569\,x)$$

> $plot((41), x = x22 .. x33)$

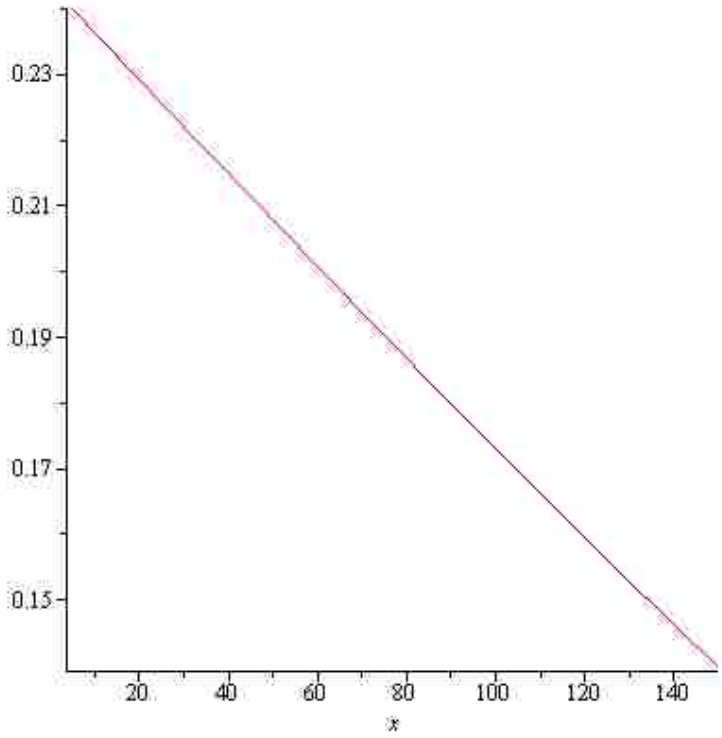

> $cc4$

$$0.1088002899 - 0.07461729972\,\mathrm{erf}(0.0007009651925\,x)$$

> $plot((42), x = x33 .. x44)$

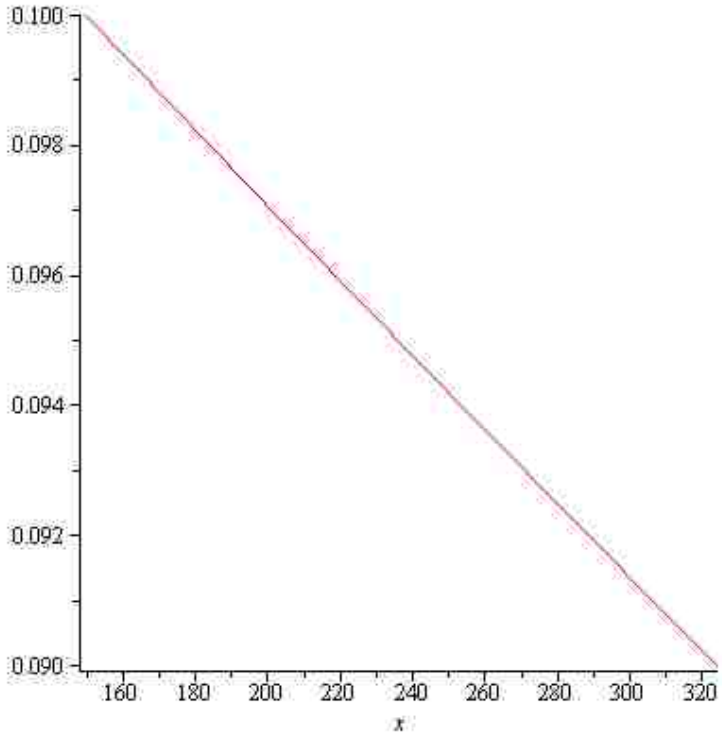

> $cc5$

$$-0.01674730336\,\mathrm{erf}(0.0002861678415\,x) + 0.01674730336$$

> $plot((43), x = x44 .. 1000)$

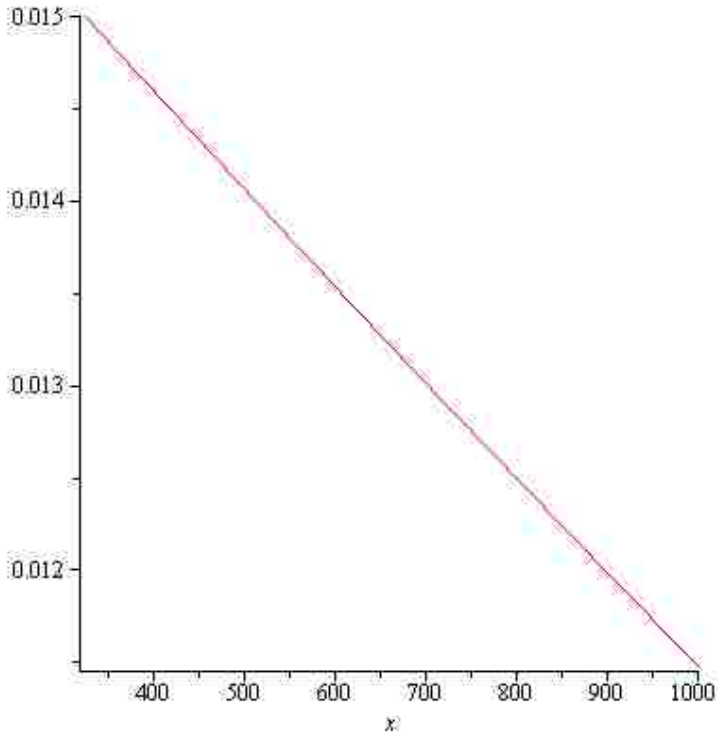

>

A.3 Maple Code for the Cu-Zn Case

> *restart*;

> $C_1 := 1; C_2 := 0.61; C_3 := 0.55; C_4 := 0.515; C_5 := 0.425; C_6 := 0.315; C_7 := 0.215; C_8 := 0.125; C_9 := 0.035; C_{10} := 0;$

$$C_1 := 1$$

$$C_2 := 0.61$$

$$C_3 := 0.55$$

$$C_4 := 0.515$$

$$C_5 := 0.425$$

$$C_6 := 0.315$$

$$C_7 := 0.215$$

$$C_8 := 0.125$$

$$C_9 := 0.035$$

$$C_{10} := 0$$

> $De := 0.67e4;$

$$De := 6700.$$

> $\gamma 1 := 15000;$

$$\gamma 1 := 15000$$

> $\gamma 2 := 2800;$

$$\gamma 2 := 2800$$

> $\gamma 3 := 121;\ \gamma 4 := 335;$

$$\gamma 3 := 121$$

$$\gamma 4 := 335$$

> $Da := \frac{De}{\gamma 1};\ Db := \frac{De}{\gamma 2};\ Dc := \frac{De}{\gamma 3};\ Dd := \frac{De}{\gamma 4}$

$$Da := 0.4466666667$$

$$Db := 2.392857143$$

$$Dc := 55.37190083$$

$$Dd := 20.00000000$$

>

> $$eqn1 := C_2 - C_3 = \frac{\left(C_4 - C_3\right) e^{-\gamma 2\, \eta_1^2}}{\eta_1 \sqrt{\pi\, \gamma 2}\ \left(-\operatorname{erf}\left(\sqrt{\gamma 2}\ \eta_1\right) + \operatorname{erf}\left(\sqrt{\gamma 2}\ \eta_2\right)\right)} - \frac{\left(C_2 - C_1\right) e^{-\gamma 1\, \eta_1^2}}{\eta_1 \sqrt{\pi\, \gamma 1}\ \operatorname{erf}\left(\sqrt{\gamma 1}\ \eta_1\right)}$$

$$eqn1 := 0.06 = -\frac{0.0002500000000\, e^{-2800\, \eta_1^2} \sqrt{7}}{\eta_1 \sqrt{\pi}\ \left(-\operatorname{erf}\left(20 \sqrt{7}\ \eta_1\right) + \operatorname{erf}\left(20 \sqrt{7}\ \eta_2\right)\right)} + \frac{0.001300000000\, e^{-15000\, \eta_1^2} \sqrt{6}}{\eta_1 \sqrt{\pi}\ \operatorname{erf}\left(50 \sqrt{6}\ \eta_1\right)}$$

> $simplify(\ \mathbf{(7)}\ )$

$$0.06000000000 = \left(4.000000000\, 10^{-13} \left(9.32940832\, 10^{8}\, e^{-2800.\, \eta_1^2} \operatorname{erf}\left(122.474487\right.\right.\right.$$
$$+ 4.491423945\, 10^{9}\, e^{-15000.\, \eta_1^2} \operatorname{erf}\left(52.91502622\, \eta_1\right)$$
$$\left.\left.\left. - 4.491423945\, 10^{9}\, e^{-15000.\, \eta_1^2} \operatorname{erf}\left(52.91502622\, \eta_2\right)\right)\right) \Big/$$
$$\left(\operatorname{erf}\left(122.4744872\, \eta_1\right) \left(\operatorname{erf}\left(52.91502622\, \eta_1\right)\right.\right.$$
$$\left.\left. - 1.\, \operatorname{erf}\left(52.91502622\, \eta_2\right)\right)\, \eta_1\right)$$

> $eqn2 := C_4 - C_5 = \dfrac{(C_6 - C_5)\, e^{-\gamma 3\, \eta_2^2}}{\eta_2 \sqrt{\pi\, \gamma 3}\, \left(-\operatorname{erf}\left(\sqrt{\gamma 3}\, \eta_2\right) + \operatorname{erf}\left(\sqrt{\gamma 3}\, \eta_3\right)\right)} - \dfrac{(C_4 - C_3)\, e^{-\gamma 2\, \eta_2^2}}{\eta_2 \sqrt{\pi\, \gamma 2}\, \left(-\operatorname{erf}\left(\sqrt{\gamma 2}\, \eta_1\right) + \operatorname{erf}\left(\sqrt{\gamma 2}\, \eta_2\right)\right)}$

$$eqn2 := 0.090 = -\frac{0.01000000000\, e^{-121\, \eta_2^2}}{\eta_2 \sqrt{\pi}\, \left(-\operatorname{erf}\left(11\, \eta_2\right) + \operatorname{erf}\left(11\, \eta_3\right)\right)} + \frac{0.0002500000000\, e^{-2800\, \eta_2^2} \sqrt{7}}{\eta_2 \sqrt{\pi}\, \left(-\operatorname{erf}\left(20 \sqrt{7}\, \eta_1\right) + \operatorname{erf}\left(20 \sqrt{7}\, \eta_2\right)\right)}$$

> *simplify*(**(9)**)

$$0.09000000000 = \left(2.000000000\, 10^{-13} \left(2.820947918\, 10^{10}\, e^{-121.\, \eta_2^2} \operatorname{erf}\left(52.915026 - 2.820947918\, 10^{10}\, e^{-121.\, \eta_2^2} \operatorname{erf}\left(52.91502622\, \eta_2\right) - 1.865881663\, 10^{9}\, e^{-2800.\, \eta_2^2} \operatorname{erf}\left(11.\, \eta_2\right) + 1.865881663\, 10^{9}\, e^{-2800.\, \eta_2^2} \operatorname{erf}\left(11.\, \eta_3\right)\right)\right) \Big/ \left(\left(\operatorname{erf}\left(52.91502622\, \eta_1\right) - 1.\, \operatorname{erf}\left(52.91502622\, \eta_2\right)\right) \left(\operatorname{erf}\left(11.\, \eta_2\right) - 1.\, \operatorname{erf}\left(11.\, \eta_3\right)\right) \eta_2\right)$$

> $eqn3 := C_6 - C_7 = \dfrac{(C_8 - C_7)\, e^{-\gamma 4 \cdot \eta_3^2}}{\eta_3 \sqrt{\pi\, \gamma 4}\, \left(-\operatorname{erf}\left(\sqrt{\gamma 4}\, \eta_3\right) + \operatorname{erf}\left(\sqrt{\gamma 4}\, \eta_4\right)\right)} - \dfrac{(C_6 - C_5)\, e^{-\gamma 3\, \eta_3^2}}{\eta_3 \sqrt{\pi\, \gamma 3}\, \left(-\operatorname{erf}\left(\sqrt{\gamma 3}\, \eta_2\right) + \operatorname{erf}\left(\sqrt{\gamma 3}\, \eta_3\right)\right)}$

$$eqn3 := 0.100 = -\frac{0.0002686567164\, e^{-335\, \eta_3^2} \sqrt{335}}{\eta_3 \sqrt{\pi}\, \left(-\operatorname{erf}\left(\sqrt{335}\, \eta_3\right) + \operatorname{erf}\left(\sqrt{335}\, \eta_4\right)\right)} + \frac{0.01000000000\, e^{-121\, \eta_3^2}}{\eta_3 \sqrt{\pi}\, \left(-\operatorname{erf}\left(11\, \eta_2\right) + \operatorname{erf}\left(11\, \eta_3\right)\right)}$$

> *simplify*(**(13)**)

$$0.09000000000 = -\left(2.256758334\,10^{-12}\,e^{-1.\,\eta_4^2}\left(-8.750000000\,10^{9}\,\mathrm{erf}\left(18.30300522\,\eta_3\right)+8.750000000\,10^{9}\,\mathrm{erf}\left(18.30300522\,\eta_4\right)-1.229306321\,10^{9}\,e^{-334.\,\eta_4^2}+1.229306321\,10^{9}\,e^{-334.\,\eta_4^2}\,\mathrm{erf}\left(\eta_4\right)\right)\right)\Big/\left(\left(\mathrm{erf}\left(18.30300522\,\eta_3\right)-1.\,\mathrm{erf}\left(18.30300522\,\eta_4\right)\right)\left(-1.+\mathrm{erf}\left(\eta_4\right)\right)\eta_4\right)$$

> $eqn4 := C_8 - C_9 = \dfrac{\left(C_{10}-C_9\right)e^{-\eta_4^2}}{\eta_4\sqrt{\pi}\,\left(1-\mathrm{erf}\left(\eta_4\right)\right)} - \dfrac{\left(C_8-C_7\right)e^{-\gamma 4\cdot\eta_4^2}}{\eta_4\sqrt{\pi\,\gamma 4}\,\left(-\mathrm{erf}\left(\sqrt{\gamma 4}\,\eta_3\right)+\mathrm{erf}\left(\sqrt{\gamma 4}\,\eta_4\right)\right)}$

$$eqn4 := 0.090 = -\frac{0.035\,e^{-\eta_4^2}}{\eta_4\sqrt{\pi}\,\left(1-\mathrm{erf}\left(\eta_4\right)\right)} + \frac{0.0002686567164\,e^{-335\,\eta_4^2}\sqrt{335}}{\eta_4\sqrt{\pi}\,\left(-\mathrm{erf}\left(\sqrt{335}\,\eta_3\right)+\mathrm{erf}\left(\sqrt{335}\,\eta_4\right)\right)}$$

> *simplify*(**(13)**)

$$0.09000000000 = -\left(2.256758334\,10^{-12}\,e^{-1.\,\eta_4^2}\left(-8.750000000\,10^{9}\,\mathrm{erf}\left(18.30300522\,\eta_3\right)+8.750000000\,10^{9}\,\mathrm{erf}\left(18.30300522\,\eta_4\right)-1.229306321\,10^{9}\,e^{-334.\,\eta_4^2}+1.229306321\,10^{9}\,e^{-334.\,\eta_4^2}\,\mathrm{erf}\left(\eta_4\right)\right)\right)\Big/\left(\left(\mathrm{erf}\left(18.30300522\,\eta_3\right)-1.\,\mathrm{erf}\left(18.30300522\,\eta_4\right)\right)\left(-1.+\mathrm{erf}\left(\eta_4\right)\right)\eta_4\right)$$

> $\{eqn1, eqn2, eqn3, eqn4\}$

$$\left\{0.06 = -\frac{0.0002500000000\,e^{-2800\,\eta_1^2}\sqrt{7}}{\eta_1\sqrt{\pi}\left(-\operatorname{erf}\left(20\sqrt{7}\,\eta_1\right)+\operatorname{erf}\left(20\sqrt{7}\,\eta_2\right)\right)}\right.$$

$$+\frac{0.001300000000\,e^{-15000\,\eta_1^2}\sqrt{6}}{\eta_1\sqrt{\pi}\,\operatorname{erf}\left(50\sqrt{6}\,\eta_1\right)}, 0.090 =$$

$$-\frac{0.01000000000\,e^{-121\,\eta_2^2}}{\eta_2\sqrt{\pi}\left(-\operatorname{erf}\left(11\,\eta_2\right)+\operatorname{erf}\left(11\,\eta_3\right)\right)}$$

$$+\frac{0.0002500000000\,e^{-2800\,\eta_2^2}\sqrt{7}}{\eta_2\sqrt{\pi}\left(-\operatorname{erf}\left(20\sqrt{7}\,\eta_1\right)+\operatorname{erf}\left(20\sqrt{7}\,\eta_2\right)\right)}, 0.090 =$$

$$-\frac{0.035\,e^{-\eta_4^2}}{\eta_4\sqrt{\pi}\left(1-\operatorname{erf}\left(\eta_4\right)\right)}$$

$$+\frac{0.0002686567164\,e^{-335\,\eta_4^2}\sqrt{335}}{\eta_4\sqrt{\pi}\left(-\operatorname{erf}\left(\sqrt{335}\,\eta_3\right)+\operatorname{erf}\left(\sqrt{335}\,\eta_4\right)\right)}, 0.100 =$$

$$-\frac{0.0002686567164\,e^{-335\,\eta_3^2}\sqrt{335}}{\eta_3\sqrt{\pi}\left(-\operatorname{erf}\left(\sqrt{335}\,\eta_3\right)+\operatorname{erf}\left(\sqrt{335}\,\eta_4\right)\right)}$$

$$\left.+\frac{0.01000000000\,e^{-121\,\eta_3^2}}{\eta_3\sqrt{\pi}\left(-\operatorname{erf}\left(11\,\eta_2\right)+\operatorname{erf}\left(11\,\eta_3\right)\right)}\right\}$$

> *fsolve*(**(15)**, {η[1] = 2.7656417e−4, η[2] = 4.65986700918e−4, η[3] = 1.7714668886e−2, η[4] = 1.9736364820e−2})

$$\{\eta_1 = 0.0004779231968, \eta_2 = 0.0007085456985, \eta_3 = 0.01774947305,$$
$$\eta_4 = 0.02350330316\}$$

> $\eta_1 := 0.0004779231968; \eta_2 := 0.0007085456985; \eta_3 := 0.01774947305; \eta_4 := 0.02350330316;$

$$\eta_1 := 0.0004779231968$$

$$\eta_2 := 0.0007085456985$$

$$\eta_3 := 0.01774947305$$

$$\eta_4 := 0.02350330316$$

> $x44 := \eta_4 \cdot \sqrt{4 \cdot De \cdot 3600 \cdot 8}$

$$x44 := 652.9689698$$

> $x33 := \eta_3 \cdot \sqrt{4 \cdot De \cdot 3600 \cdot 8}$

$$x33 := 493.1160124$$

> $x22 := \eta_2 \cdot \sqrt{4 \cdot De \cdot 3600 \cdot 8}$

$$x22 := 19.68482267$$

> $x11 := \eta_1 \cdot \sqrt{4 \cdot De \cdot 3600 \cdot 8}$

$$x11 := 13.27766635$$

> $DD1 := \dfrac{(C_2 - C_1)}{\operatorname{erf}\left(\sqrt{\gamma 1}\ \eta_1\right)} \cdot \operatorname{erf}\left(\sqrt{\gamma 1}\ \eta\right)$

$$DD1 := -\frac{0.39 \operatorname{erf}\left(50\sqrt{6}\ \eta\right)}{\operatorname{erf}\left(0.02389615984\sqrt{6}\right)}$$

> $c1 = C_1 + DD1$

$$c1 = 1 - \frac{0.39 \operatorname{erf}\left(50\sqrt{6}\ \eta\right)}{\operatorname{erf}\left(0.02389615984\sqrt{6}\right)}$$

> $solve(\ \mathbf{(23)}, c1\ )$

$$1.000000000 - 5.911552743 \operatorname{erf}(122.4744871\ \eta)$$

> $cc1 := solve(\ \mathbf{(23)}, c1\ )$

$$cc1 := 1.000000000 - 5.911552743 \operatorname{erf}(122.4744871\ \eta)$$

> $plot\left([cc1], \eta = 0..\eta_1\right)$

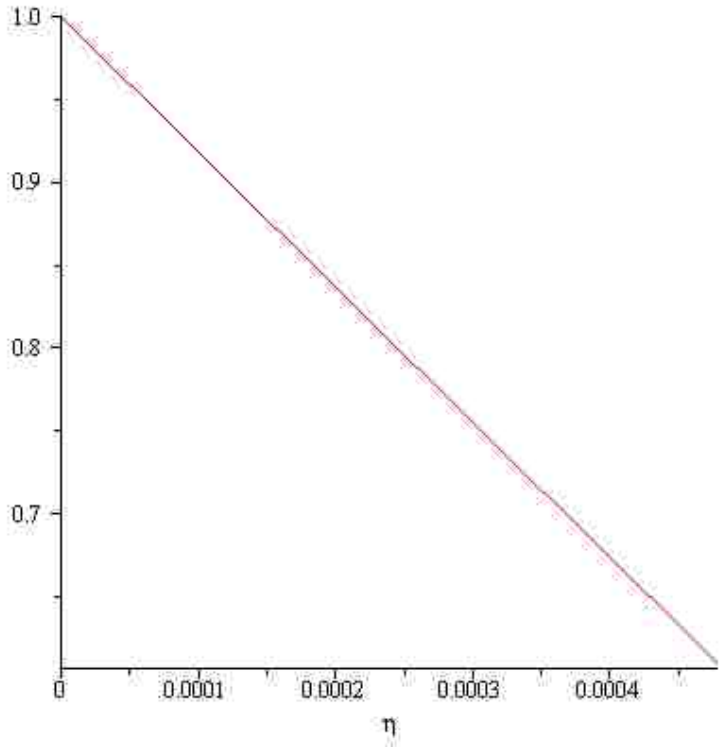

> $DD2 := \frac{(C_4 - C_3)}{-\mathrm{erf}\left(\sqrt{\gamma 2}\,\eta_1\right) + \mathrm{erf}\left(\sqrt{\gamma 2}\,\eta_2\right)} \cdot \left(\mathrm{erf}\left(\sqrt{\gamma 2}\,\eta\right) - \mathrm{erf}\left(\sqrt{\gamma 2}\,\eta_1\right)\right)$

$$DD2 := -\frac{0.035\left(\mathrm{erf}\left(20\sqrt{7}\,\eta\right) - \mathrm{erf}\left(0.009558463936\sqrt{7}\right)\right)}{-\mathrm{erf}\left(0.009558463936\sqrt{7}\right) + \mathrm{erf}\left(0.01417091397\sqrt{7}\right)}$$

> $c2 = C_3 + \mathrm{DD2}$

$$c2 = 0.55 - \frac{0.035\left(\mathrm{erf}\left(20\sqrt{7}\,\eta\right) - \mathrm{erf}\left(0.009558463936\sqrt{7}\right)\right)}{-\mathrm{erf}\left(0.009558463936\sqrt{7}\right) + \mathrm{erf}\left(0.01417091397\sqrt{7}\right)}$$

> $cc2 := solve(\ \mathbf{(27)}, c2\ );$

$$cc2 := 0.6225880668 - 2.544284203\,\mathrm{erf}\left(52.91502622\,\eta\right)$$

> $plot\left([cc2], \eta = \eta_1 .. \eta_2\right)$

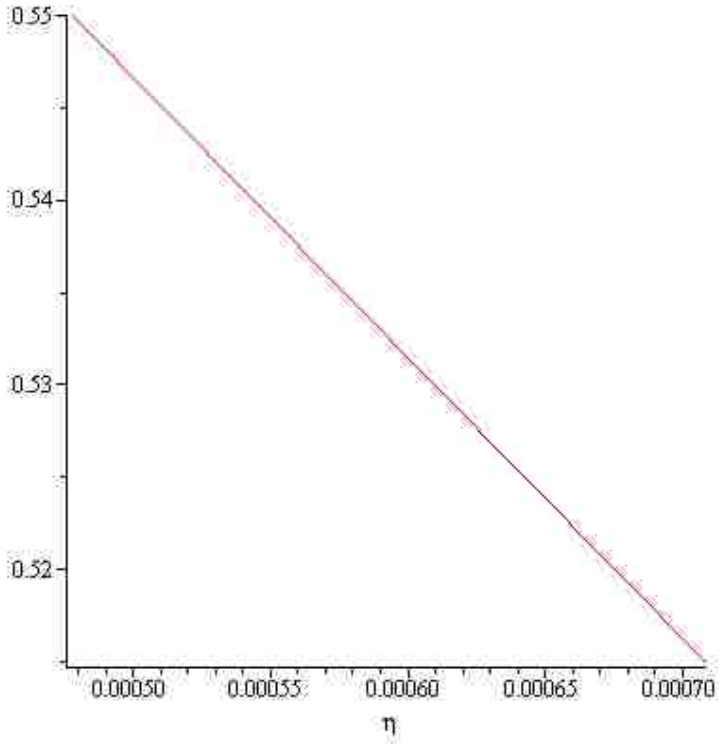

> $DD3 := \frac{(C_6 - C_5)}{-\mathrm{erf}\left(\sqrt{\gamma 3}\,\eta_2\right) + \mathrm{erf}\left(\sqrt{\gamma 3}\,\eta_3\right)} \cdot \left(\mathrm{erf}\left(\sqrt{\gamma 3}\,\eta\right) - \mathrm{erf}\left(\sqrt{\gamma 3}\,\eta_2\right)\right)$

$$DD3 := -0.5269527104\,\mathrm{erf}\left(11\,\eta\right) + 0.004634239335$$

> $c3 = C_5 + \mathrm{DD3}$

$$c3 = 0.4296342393 - 0.5269527104\,\mathrm{erf}\left(11\,\eta\right)$$

> $cc3 := solve(\ \mathbf{(30)}, c3);$

$$cc3 := 0.4296342393 - 0.5269527104\,\mathrm{erf}\left(11.\,\eta\right)$$

> $plot([cc3], \eta = \eta_2 .. \eta_3)$

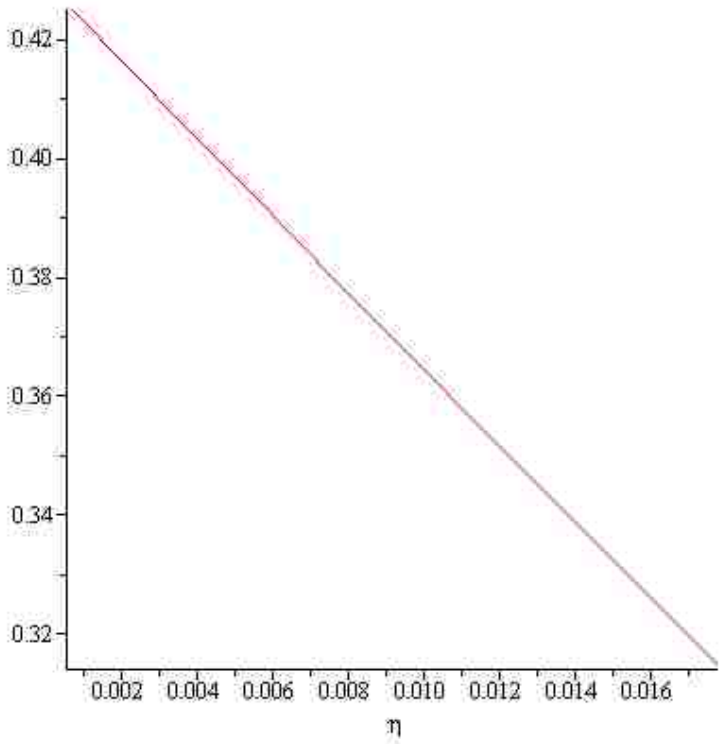

> $DD4 := \frac{(C_8 - C_7)}{-\mathrm{erf}(\sqrt{\gamma 4}\,\eta_3) + \mathrm{erf}(\sqrt{\gamma 4}\,\eta_4)} \cdot \left(\mathrm{erf}(\sqrt{\gamma 4}\,\eta) - \mathrm{erf}(\sqrt{\gamma 4}\,\eta_3)\right)$

$$DD4 := -\frac{0.090\left(\mathrm{erf}(\sqrt{335}\,\eta) - \mathrm{erf}(0.01774947305\sqrt{335})\right)}{-\mathrm{erf}(0.01774947305\sqrt{335}) + \mathrm{erf}(0.02350330316\sqrt{335})}$$

> $c4 = C_7 + DD4$

$$c4 = 0.215 - \frac{0.090\left(\mathrm{erf}(\sqrt{335}\,\eta) - \mathrm{erf}(0.01774947305\sqrt{335})\right)}{-\mathrm{erf}(0.01774947305\sqrt{335}) + \mathrm{erf}(0.02350330316\sqrt{335})}$$

> $cc4 := solve(\ \mathbf{(33)}, c4\ )$

$$cc4 := 0.5244502236 - 0.8739624313\,\mathrm{erf}(18.30300522\,\eta)$$

> $plot([cc4], \eta = \eta_3 .. \eta_4)$

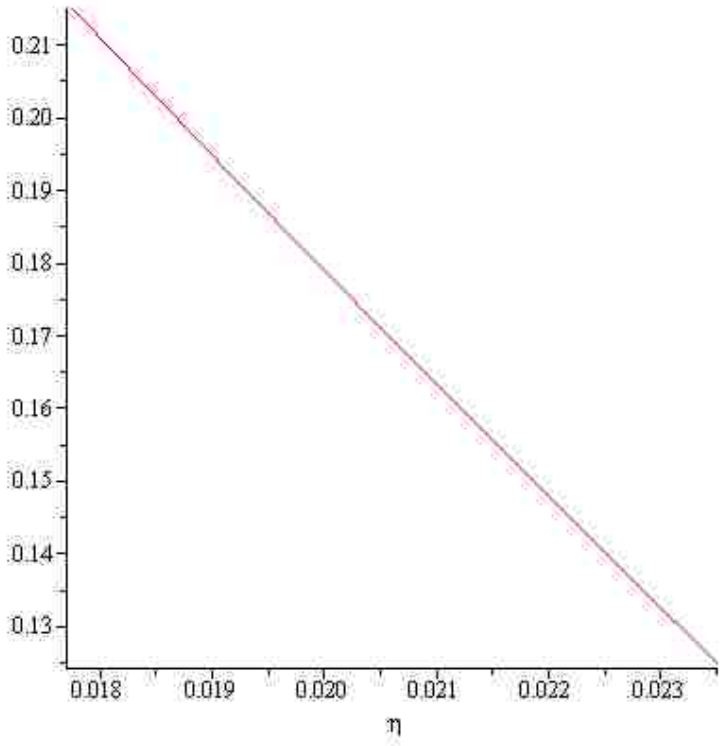

>

> $DD5 := \dfrac{2\cdot\left(C_{10}-C_9\right)}{\sqrt{\pi}\cdot\left(1-\operatorname{erf}\left(\eta_4\right)\right)}$

$$DD5 := -\frac{0.07190665936}{\sqrt{\pi}}$$

> $c5 = -DD5\cdot\int_{\eta}^{\infty} e^{-\eta^2}\,d\eta$

$$c5 = \frac{0.07190665936\left(-\frac{1}{2}\sqrt{\pi}\,\operatorname{erf}(\eta)+\frac{1}{2}\sqrt{\pi}\right)}{\sqrt{\pi}}$$

> $cc5 := solve(\ \mathbf{(36)}, c5)$

$$cc5 := -0.03595332968\,\operatorname{erf}(\eta)+0.03595332968$$

> $plot\left([cc3], \eta = \eta_2..\eta_3\right)$

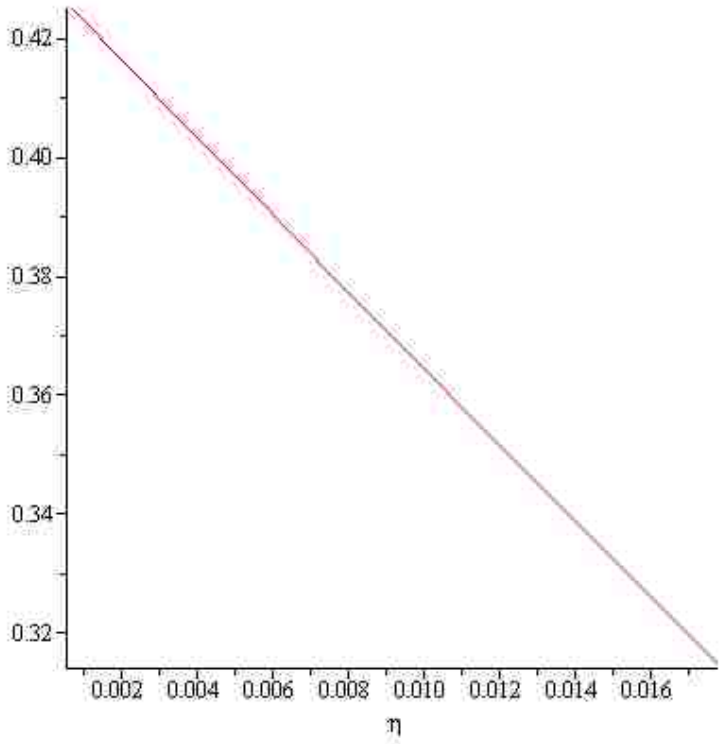

> $DD4 := \dfrac{(C_8 - C_7)}{-\operatorname{erf}\left(\sqrt{\gamma 4}\ \eta_3\right) + \operatorname{erf}\left(\sqrt{\gamma 4}\ \eta_4\right)} \cdot \left(\operatorname{erf}\left(\sqrt{\gamma 4}\ \eta\right) - \operatorname{erf}\left(\sqrt{\gamma 4}\ \eta_3\right)\right)$

$$DD4 := -\frac{0.090\left(\operatorname{erf}\left(\sqrt{335}\ \eta\right) - \operatorname{erf}\left(0.01774947305\sqrt{335}\right)\right)}{-\operatorname{erf}\left(0.01774947305\sqrt{335}\right) + \operatorname{erf}\left(0.02350330316\sqrt{335}\right)}$$

> $c4 = C_7 + DD4$

$$c4 = 0.215 - \frac{0.090\left(\operatorname{erf}\left(\sqrt{335}\ \eta\right) - \operatorname{erf}\left(0.01774947305\sqrt{335}\right)\right)}{-\operatorname{erf}\left(0.01774947305\sqrt{335}\right) + \operatorname{erf}\left(0.02350330316\sqrt{335}\right)}$$

> $cc4 := solve(\ \mathbf{(33)}, c4\ )$

$$cc4 := 0.5244502236 - 0.8739624313\operatorname{erf}\left(18.30300522\,\eta\right)$$

> $plot\left([cc4], \eta = \eta_3 .. \eta_4\right)$

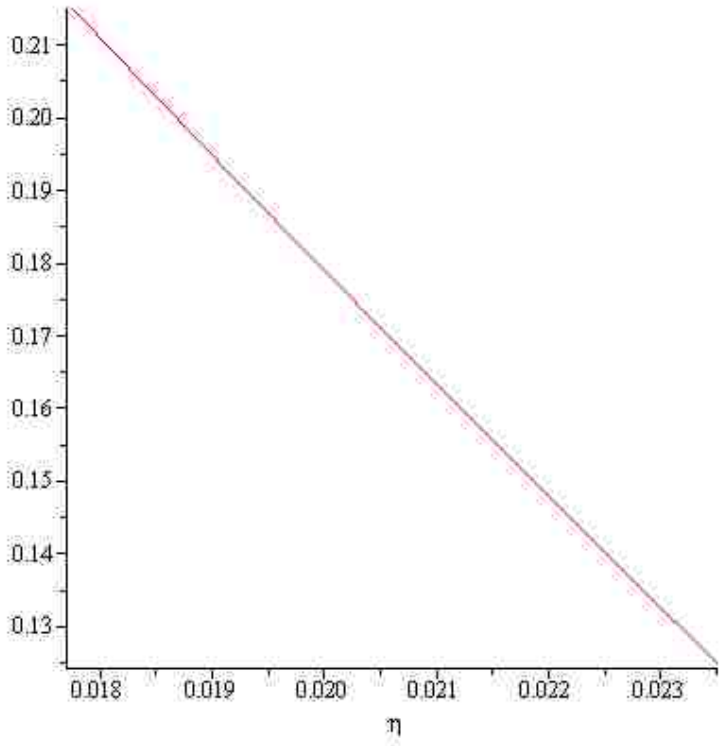

>

> $DD5 := \dfrac{2\cdot\left(C_{10}-C_9\right)}{\sqrt{\pi}\cdot\left(1-\operatorname{erf}\left(\eta_4\right)\right)}$

$$DD5 := -\frac{0.07190665936}{\sqrt{\pi}}$$

> $c5 = -DD5\cdot\int_{\eta}^{\infty} e^{-\eta^2}\,d\eta$

$$c5 = \frac{0.07190665936\left(-\frac{1}{2}\sqrt{\pi}\,\operatorname{erf}(\eta)+\frac{1}{2}\sqrt{\pi}\right)}{\sqrt{\pi}}$$

> $cc5 := solve(\ (36), c5)$

$$cc5 := -0.03595332968\,\operatorname{erf}(\eta)+0.03595332968$$

> $plot(\ (42), x = x33\ldots x44)$

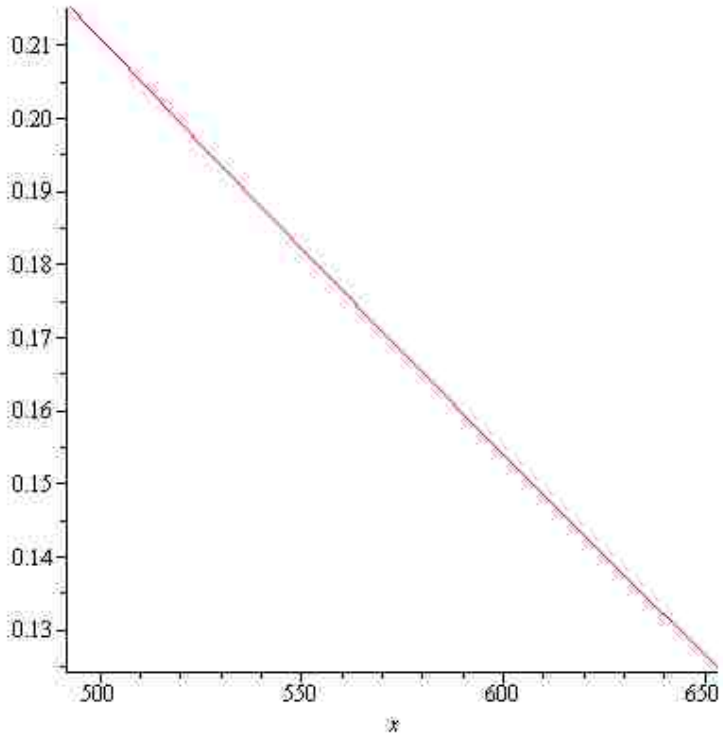

> *cc5*

$$-0.03595332968\,\mathrm{erf}(0.00003599451773\,x) + 0.03595332968$$

> *plot*((**43**), $x = x44 .. 100000$)

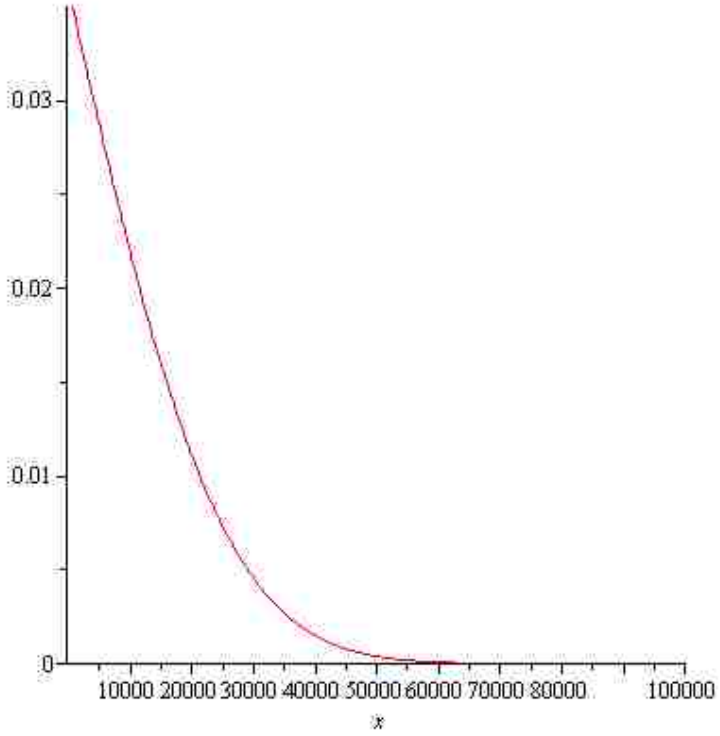

>

VITA

Bandar Alzahrani was born on May 27, 1979 in Alhokman; a village in the southern region of Saudi Arabia. He is the second son of Abdulrahman and Salehah. He is married to Nada Alzahrani and he has two daughters Jawan and Lara. He acquired Bachelor degree in Mechanical Engineering in 2001 from King Abdulaziz University with Excellent GPA and second honor. In 2002, he got a job as a material engineer at Saudi Electricity Company and worked there for more than six years. In 2008, he joined King Saud University as a teaching assistant in the university branch at Alkharj. In 2009, he entered Lehigh University to get Master of Science degree in mechanical Engineering. Presently, He is looking forward to pursue his doctoral degree in manufacturing field.